공학박사학위논문

도로 노면 상태 업데이트 및 인공 조향 모델을 활용한 스티어 바이 와이어 시스템 햅틱 제어

Artificial Steering Model based Haptic Control of Steer by Wire System with Tire-Road Condition Parameter Update

2021년 2월

서울대학교 대학원

기계항공공학부

이 재 풍

도로 노면 상태 업데이트 및 인공 조향 모델을 활용한 스티어 바이 와이어 시스템 햅틱 제어

Artificial Steering Model based Haptic Control of Steer by Wire System with Tire-Road Condition Parameter Estimation

지도교수 이 경 수

이 논문을 공학박사 학위논문으로 제출함

2020 년 10 월

서울대학교 대학원

기계항공공학부

이 재 풍

이재풍의 공학박사 학위논문을 인준함

2020 년 12 월

위 원 장 : 차 석 원 (인)

부위원장 : 이 경 수 (인)

위 원 : 박 용 래 (인)

위 원 : 신 동 훈 (인)

위 원 : 오 광 석 (인)

Abstract

Artificial Steering Model based Haptic Control of Steer by Wire System with Tire-Road Condition Parameter Update

Jaepoong Lee

School of Mechanical and Aerospace Engineering

The Graduate School

Seoul National University

With the development of autonomous driving technology, many vehicle manufacturers are developing steering systems suitable for autonomous driving. Until recently, Electric-Power-Steering Systems (EPS) has been used because of its advantages of lower weight and lower energy consumption than Hydraulic Power Steering systems (HPS). However, since both steering systems are connected by mechanical linkages, these systems are not suitable for implementing autonomous driving technology. The continuous mechanical linkage has been eliminated in Steer-by-wire (SBW) vehicles using X-by-wire technology to the steering system. The SBW system improves convenience and safety when implementing autonomous driving technology by operating the rack system and steering system independently. Strategies for fail-safe are required to ensure the stability of the overall system.

Various studies have been conducted to develop the SBW system. The studies of the SBW system are largely divided into three areas: artificial steering feel generation of steering wheel system, rack position tracking, system fail safe. In SBW system, since there is no mechanical linkage, the steering reaction torque is not transmitted from the tire, so the artificial steering feel should be generated. Also, the position of the tire should be controlled according to the steering input applied by the driver.

This dissertation focused on designing a haptic control algorithm to render artificial steering feel. An angle sensor was installed in the steering wheel system to generate artificial steering feel based on the steering wheel angle. Using the vehicle states and the steering states estimated through the measured steering wheel angle, the artificial steering feel was designed. The parameters of the rack system were estimated to transmit the road surface information to the driver. This online parameter estimation of rack system lateral load model was used to update the designed artificial steering feel. However, there are some cases in which the steering wheel system becomes unstable due to sensor quantization and sampling rate. Unintentional behavior such as limit cycles occur in unstable rendering models. Through passivity analysis, the passivity of the rendering model which is the artificial steering feel was determined. When the passivity condition is satisfied, the parameters have been updated to transmit road surface information to the driver.

The proposed haptic control algorithm was evaluated by conducting computer simulation and vehicle test under various steering conditions and road surface conditions. The proposed passivity conditions were also validated by computer simulation. The test results show that the performances of haptic rendering were successfully achieved by the proposed haptic control algorithm.

Keywords: Steer-by-wire, Haptic Control, Steering Feel, Vehicle Chassis Control, Steering System, Steering Wheel System, Parameter Estimation, Passivity Analysis, Limit Cycle.

Student Number: 2017-30011

List of Figures

Contents

Chapter 1 Introduction

1.1. Background and Motivation

The steering system converts the rotation of the steering wheel into a road wheel. Since rotating the road wheel directly requires too much torque, the steering system has a gearbox. Using a gear box has the effect of reducing torque, although steering wheel angle need to be turned more. The driver's torque is transmitted to the road wheel through the steering wheel, steering column, universal joint, rack and pinion gear, and tie rod. However, as the weight of the vehicle increases, it is inefficient to use the gear box to reduce the driver's torque. Therefore, to reduce steering effort, additional actuators are used to reduce the driver's torque. A steering system using additional actuators is called a power steering system. The power steering system has been developed into Hydraulic power steering systems (HPS), Electro-hydraulic power steering systems (EHPS), and Electric power steering systems (EPS).

In the hydraulic power steering systems, the hydraulic pressure generated by the engine power is used to assist the driver in turning the front wheels(Stolte 1957). It is a steering system that has been used for a long time and is evaluated for its excellent steering feel. However, it has the disadvantage of reducing the engine power. To compensate for this disadvantage, a motor, not an engine, is used to generate hydraulic pressure in electro-hydraulic power steering systems (Kokotovic, Grabowski et al. 1999) (Suzuki, Inaguma et al. 1995). This system has good steering feel and improves fuel efficiency, but it has the disadvantages of complicated structure and increased price. In electric power steering systems, there is no hydraulic system with a complicated structure (Shimizu 1989). This system generates assist torque directly using a motor. The simple structure of the steering system saves space and reduces weight. Since the assist torque is generated based on the driver's torque measured by the torque sensor, the response speed is slow and the steering feel is not good compared to the hydraulic power steering system (Kim and Song 2002).

In addition to reducing the driver's effort, various studies have been conducted to ensure vehicle stability such as active front steering system. The active front steering system uses a planetary gear to additionally steer the road wheel (Klier, Reimann et al. 2004). Various studies have been conducted to determine additional road wheel angle in consideration of vehicle stability (Nam, Fujimoto et al. 2012). Furthermore, studies were conducted on integrated control algorithms using various chassis modules such as brake and in-wheel-motor (Di Cairano, Tseng et al. 2012) (Falcone, Eric Tseng et al. 2008) (Ren, Chen et al. 2016).

In recent years, research on steer-by-wire which has introduced X-by-Wire technology, has been actively conducted. In steer-by-wire system, unlike conventional steering systems, steering wheel and road wheel are not connected by mechanical linkages. Using various sensors and motors, the steering wheel and road wheel are separated (Kaufmann and Byers 2002). Because mechanical linkage has been removed, it can save more space than electric power steering system and it is also lighter in weight. Also, because road wheel angle is directly controlled, vehicle stability can be ensured like active front steering system (Zheng and Anwar 2009) (Zheng and Lenart 2006). Furthermore, steer-by-wire is a steering system suitable for implementing autonomous driving technology. When autonomous driving technology is implemented in conventional steering systems, the steering wheel can be continuously moved and unnecessary steering input can be applied from driver. On the other hand, each system is separated independently in steer-by-wire. When autonomous driving is performed, the steering wheel can be stopped and the effect of the steering input can be neglected (Gazit 2015).

However, steer-by-wire system has a poorer steering feel than electric power steering system. In conventional power steering systems, the actuators assist the driver to steer because the road wheel generates a large reaction force. On the other hand, in steer-by-wire, the reaction force of the road wheel is not transmitted, so an artificial reaction force must be generated by the actuator. Various studies were conducted using magnetorheological fluid to generate the steering reaction torque (Ahmadkhanlou, Washington et al. 2006) (Peretti and Zigliotto 2006) (Park and Jung 2001). A magnetorheological fluid has a low price but a semi-active characteristic.

Therefore, in this dissertation, a haptic control algorithm that generates the steering feel of the driver using permanent magnet synchronous motor is proposed.

1.2. Previous Researches

Over the past few decades, research on steering feel has been conducted on various steering systems. The study on hydraulic power steering system focuses on reducing driver efficiency while consuming less energy (Rogers, Speer et al. 2003). Even recently, the hydraulic power steering systems have been the benchmark for good steering feel. The electric power steering system, which uses a motor to generate assist torque, is evaluated as having a poorer steering feel than the hydraulic power steering system. Since then, research on steering feel was actively conducted. The electric power steering system is classified into column type, pinion type, and rack type according to the mounting position of the motor. The closer the motor is mounted to the driver, the more the noise and torque ripple generated by the motor affect the driver (Badawy, Zuraski et al. 1999). Although the steering feel is not good, column type electric power steering system, which is inexpensive, has been installed in many vehicles. Therefore, studies have been conducted to compensate for torque ripple (Collier-Hallman and Chandy 2000) (Boules, Henry et al. 2002). In addition, algorithms have been developed to compensate for the phase delay caused by mounting away from the road wheel (Noro, Hironaka et al. 1997) (Kobayashi, Sakaguchi et al. 2011).

Unlike the conventional steering system that generates assist torque, the steer-by-wire system has to generate an artificial steering reaction torque. The steer-by-wire systems using inexpensive magnetorheological fluids were also studied on the steering feel (Peretti and Zigliotto 2006). However, most commercially available steer-by-wire vehicles utilize a motor to generate steering reaction torque (Discenzo 2000). Therefore, in this dissertation, a study was conducted to generate the steering feel of a steer-by-wire vehicle using a motor.

The objective of most recent studies is to control the motor in a steering system of steer-by-wire that is most similar to the conventional steering systems such as electric power steering and hydraulic power steering (Odenthal, Bünte et al. 2002). Oh assumed the steering feel of the conventional steering system as a map based on the steering angle and steering angular velocity (Oh, Chae et al. 2004). Asai suggested steering feel based on the position of the road wheel and transmitted the road disturbance to the driver (Asai, Kuroyanagi et al. 2004). A Balachandran proposed the steering feel based on the dynamic model of the vehicle (Balachandran and Gerdes 2014). P. Seflur proposed a methodology for generating the steering feel by synchronizing the steering system including the steering wheel and the rack system including the road wheel (Setlur, Wagner et al. 2006). K.Scicluna suggested a method of directly controlling the tree-phase current input of permanent magnet synchronous motor, not designing the steering feel (Scicluna, Staines et al. 2017). Fanken proposed a method of generating the steering feel based on rack force in order to transmit the road reaction torque to the driver(Fankem and Müller 2014).

Not only the feedforward method but also the feedback method based on the driver’s torque has been studied in various way (Radamis and Zheng 2003). To design the feedback control algorithm, a torque sensor was installed in the steer-by-wire system. X Wu designed a bilateral feedback control algorithm including rack system. (Wu, Ye et al. 2016)

Studies were also conducted to design a feedback algorithm without mounting a torque sensor. DS cheon designed a torque sensor-less feedback control algorithm using a disturbance observer (Cheon and Nam 2017). N. Bajcinca designed a control algorithm based on disturbance observer and active observer (Bajçinca, Cortesao et al. 2003) .

Previously, I did a study to design a feedback algorithm using a torque sensor. A feedback algorithm was designed using the impedance steering reaction torque model (Lee, Chang et al. 2017) (Lee, Kim et al. 2018). The feedback algorithm reduced the error between the driver's torque and the desired torque by using the adaptive sliding mode control methodology. However, the algorithm based on torque error does not guarantee convergence in the hands-off simulation. Therefore, an angle error-based admittance control algorithm was designed (Lee, Yi et al. 2020). Figure 1.1 shows a block diagram of the admittance control algorithm.

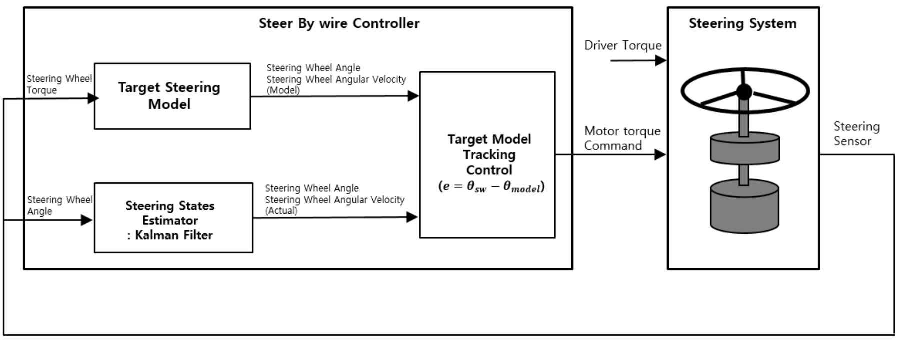

Figure 1.1 Overall block diagram of the admittance control algorithm

According to the research results of the above paper, the tracking performance for various steering models was validated in hardware-in-the-loop simulation. Figure 1.2 is the flip test results for the two different target steering models.

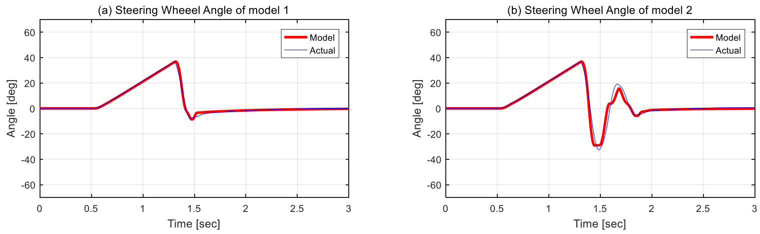

Figure 1.1 Flip test results at 70kph

However, in vehicle tests, the previously proposed algorithm was not suitable for generating the steering feel. The first reason was to design an admittance control algorithm using a target steering model that did not consider road surface information. Forsyth argued that the steering feel has a major impact on vehicle driving stability (Forsyth and MacLean 2005). Nybacka also argued that steering feel affects handling performance (Nybacka, He et al. 2014). Therefore, it is necessary to consider the road surface condition in the target steering model of the previously proposed algorithm.

Another problem with the previously proposed algorithm is that sensor performance is not considered. In the steer-by-wire system, there are torque and angle sensors to measure the driver’s steering input. Each sensor has measurement error due to quantization and sampling rate. Although the previously proposed algorithm has proven steering angle convergence, high-frequency torque can be transmitted to the driver. Especially when auxiliary sensors for fail-safe are used, the above disturbance is generated more due to the low performance of the sensors. This disturbance can also cause limit cycles and divergence. Therefore, when designing the haptic control algorithm, the specification of the sensor such as quantization and sampling rate must be considered.

In the field of haptic rendering, various haptic control algorithms considering sensor performance have been studied. N Diolaiti proposed a region of stiffness models that can be rendered using a haptic device which is a secondary system (Diolaiti, Niemeyer et al. 2005). JJ Gil proposed a region of damping and stiffness coefficient that can be rendered using the Routh-Hurwitz criterion(Gil, Sánchez et al. 2009) (Gil, Avello et al. 2004). N Colonnese proposed a region of damping and stiffness coefficient that can be rendered according to touch characteristics of human (Colonnese and Okamura 2016). In this paper, a describing function was used to analyse the generation of the limit cycles, but the calculation was complicated to analyse the damping coefficient. Therefore, they derived the passivity conditions using energy analysis and proposed render-able region. In order to analyse the limit cycle of the sampled data control system, there is a method such as hopf bifurcation, but the calculation is complicated (Zhang and Stepan 2020).

1.3. Thesis Objectives

This dissertation proposes a haptic control algorithm for generating the steering feel of the steer-by-wire system. In this dissertation, a permanent magnet synchronous motor is installed to the steering system to generate the steering feel. The motor control algorithm consists of an impedance control, parameter estimation and parameter update.

The impedance control algorithm was designed in consideration of the driver's subjective such as steering effort, steering stiffness, solid feel and centering feel(Dang, Chen et al. 2014) . The objective is to design an impedance model that satisfies the subjective and objective evaluation index. The impedance model consists only of the states of the steering system.

Therefore, to update the parameter of the impedance model, the parameters of the rack system including the road wheel is estimated. Because the tire force varies according to the road surface conditions, the objective of this dissertation is to estimate the road surface conditions though the tire force. The road surface conditions can be transmitted to the driver by reflecting the parameter on the steering feel.

However, it is not possible to update parameters in the impedance model in all situations. It is essential to derive the passivity conditions of the steering system during haptic rendering. Based on these conditions, this objective of dissertation is to design a parameter update algorithm.

1.4. Thesis Outline

This dissertation is structured in the following manner. The overall architectures of steer-by-wire system and proposed haptic control algorithm is described in Chapter 2. Chapter 3 presents the design of artificial steering feel. An impedance steering torque model which is the artificial steering feel was designed in consideration of tire dynamics according to vehicle speed. Chapter 4 describes the parameter estimation of rack system lateral load model. The dynamic equation of the rack system is derived and the online parameter estimation is designed using Kalman Filter. The rack system control algorithm required for estimation was also designed using adaptive sliding mode control (Kim, Lee et al. 2020) .

In chapter 5, the passivity analysis of the haptic device was conducted. The passivity conditions were derived by analyzing the energy of stiffness, damping, and friction rendering models. Based on this passivity conditions, Chapter 6 proposes the haptic control algorithm. When the passivity of steering system is guaranteed, the estimated parameters are updated to the haptic control algorithm. Chapter 7 presents the computer simulation test results to evaluate the passivity conditions. Also, the performance of the haptic control algorithm was evaluated based on the computer simulation and vehicle test under various road conditions. Then the conclusion which consists the summary and contribution of the proposed algorithm and future works is presented in Chapter 8.

Chapter 2 Overall Architecture

2.1 Steer-by-wire System Configuration

The Steer-by-wire system is separated into the steering system and the rack system by removing mechanical linkage. The steering system needs an actuator to generate the steering feel. A steering system configuration using magnetorheological fluid or motor is adopted. Figure 2.1 shows the configuration of the MR-damper using magnetorheological fluid.

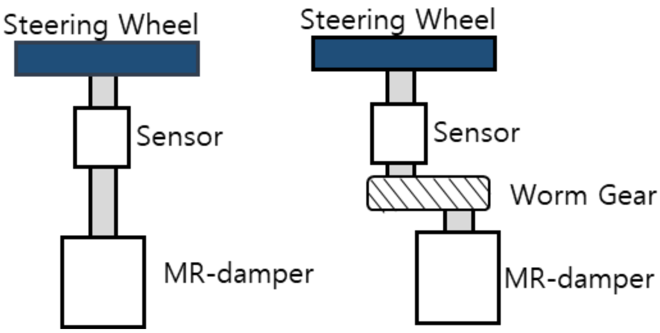

Figure 2.1 Confiugurations of steering wheel system using MR-damper

Depending on the capacity of the MR-damper, a configuration that amplifies the torque using gear is used. The MR-damper has a semi-passive characteristic, so it is difficult to generate the target torque (Ahmadkhanlou, Washington et al. 2006). Using the Bouc-Wen model, the dynamics of MR-damper is expressed as follows:

$$f = c\dot{x} + kx + \alpha z - f_0$$
$$\dot{z} = \delta\dot{x} - \beta\dot{x}|z|^n - \gamma|\dot{x}||z|^{n-1} \qquad (2.1)$$

Where f is the damping force, c is the viscous coefficient, k is the stiffness, $\dot{x}, x$ are the damper velocity and displacement, α is a scaling factor, z is the hysteretic variable and f_0 is the initial damper displacement contributing to the force offset (Spencer Jr, Dyke et al. 1997). Figure 2.2 shows that simulation result of the characteristics of MR-damper.

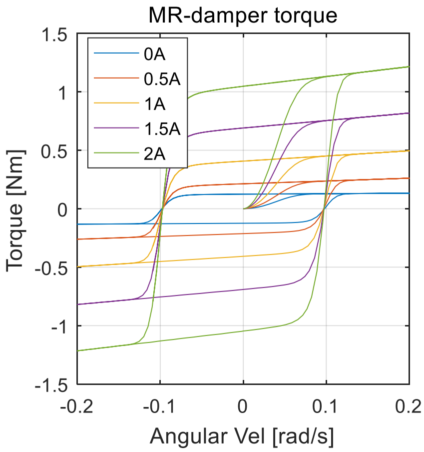

Figure 2.2 Simulation Result of MR-damper

Output torque of the MR-damper is controlled according to the magnitude of current, but it is difficult to control because the angular velocity affects the torque. Therefore, in this dissertation, a steering system is constructed using a motor which is easy to control.

Configurations using a motor are also classified according to gear mounting. The electric power steering system which is a conventional steering system, required a large magnitude of assist torque to reduce the effect of lateral tire force. Therefore, in the case of the electric power steering system, the motor torque was amplified by using the gear box such as the worm gear. When gear is used, mechanical delay is increased and backlash occurs. In addition, when the torque is amplified by gear box, the torque ripple of the motor is also amplified and transmitted to the driver. Figure 2.3 shows the simulation results of the effect of torque ripple on torque hysteresis.

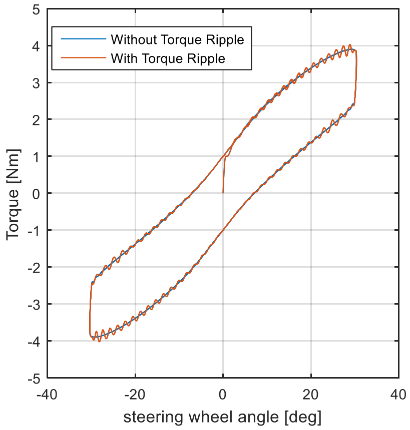

Figure 2.3 Simulation with torque ripple

However, since the steer-by-wire system generate an artificial steering feel, the range of the torque is low. Therefore, the gear box was not used in this dissertation. Figure 2.4 shows the configuration of the steering system used in this dissertation.

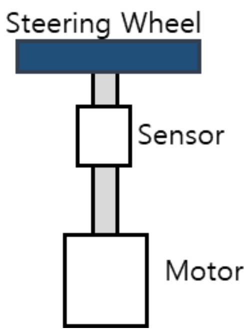

Figure 2.4 Confiugurations of steering system using motor

The motor used is a permanent magnet synchronous motor. Since the motor was directly connected to the steering wheel, it was assumed that the torque ripple phenomenon could be neglected in this dissertation. In addition, the three-phase current control algorithm was not designed. It is assumed that the torque output can be directly controlled. The sensor measured only the steering angle and the feedforward algorithm based on steering angle was designed. As shown in equation 2.2, the dynamics of the steering system is assumed to be the second-order system, and motor torque and driver torque are applied.

$$J_s\ddot{\theta}_{sw} + B_s\dot{\theta}_{sw} + F_s \,\mathrm{sgn}\left(\dot{\theta}_{sw}\right) + T_{mot} = T_{sw} \quad (2.2)$$

Where $J_s, B_s\ and\ F_s$ are the inertia, damping and friction coefficients of the steering system; T_{sw} is steering wheel torque which is driver torque input; T_{mot} is motor torque.

The steering system is continuous, but the output torque of motor is discrete according to the sampling time. The analysis of motor torque according to sampling time is presented in Chapter 5.

2.2. Haptic Control Algorithm Architecture

The haptic control algorithm is an algorithm that generates the artificial steering feel of the steering system for the driver. The haptic algorithm consists of 4 parts: Artificial Steering Model (Zero / Low / Medium to High speed), Parameter estimation of rack system lateral load model, Parameter update algorithm, Feedforward Impedance Control. Figure 2.5 shows the haptic control algorithm architecture.

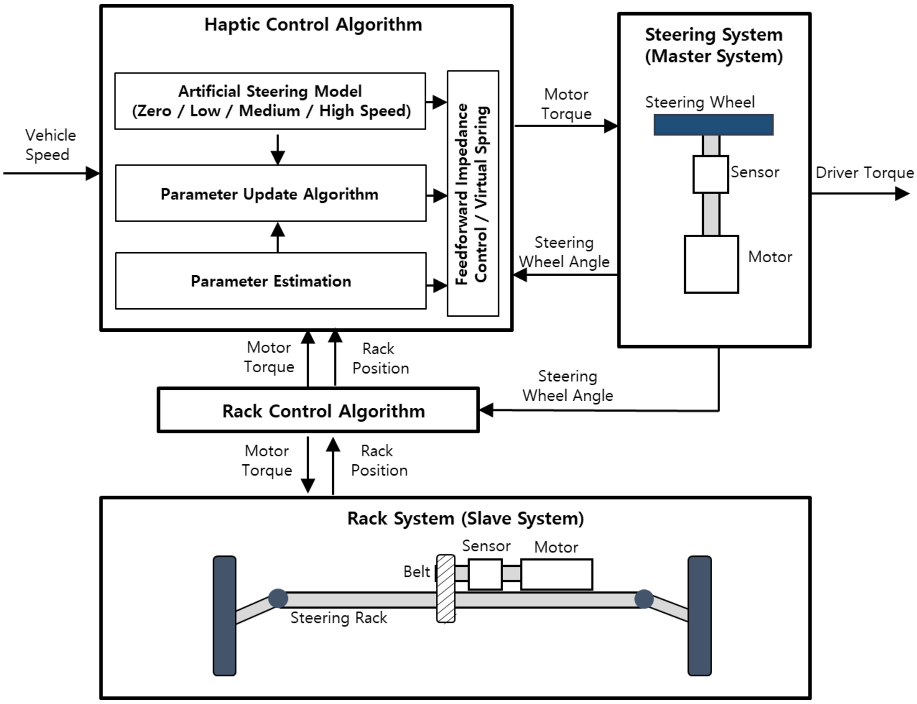

Figure 2.5 Haptic control algorithnm architecture

The first part, the artificial steering model, defines the nominal steering system model. Vehicle has different lateral tire dynamics depending on the speed, so various steering models were designed for each speed. In this part, the impedance model of the steering system according to the vehicle speed is output.

The second part, parameter estimation, estimates road surface information through the rack system. The parameters of the rack system are estimated by using the torque of rack system motor and rack position.

The third part is to update the estimated parameters to the artificial steering model. The artificial steering model is updated based on the passivity conditions derived through energy analysis. The parameter update is not conducted at low vehicle speed.

The last is the part that controls the motor based on the artificial steering model reflecting the road surface information. Since this dissertation uses a low specification sensor, the artificial steering model is rendered through feedforward control. In addition, a rack position error term was added to the control input in order to transmit the high-frequency impact on the tire to driver as shown in Chapter 6.2.

Chapter 3 Design of Artificial Steering Model

The steering feel is defined by the lateral tire dynamics. Various researchers have conducted research on the tire dynamics. The most widely used is the Magic Formula, an empirical tire model including five parameters (Pacejka and Bakker 1992). The brush tire model relies on the assumption that the slip is caused by deformation of the rubber material between the tire carcass and the ground (Pacejka 1995). These tire models are modeled based on the slip angle. In most papers, the slip angle is calculated based on the bicycle model (Sierra, Tseng et al. 2006). However, the bicycle model cannot present the stopping situation because the velocity term is in the denominator. Therefore, J. E. Bernard introduced different tire models depending on the speed (Bernard and Clover 1995).

In this paper, an artificial steering model was constructed according to the vehicle speed, taking into account that the tire characteristics vary according to the vehicle speed. The artificial steering model consists of three models according to the speed range: Zero-speed ($0kph$), Low-speed ($0\sim10kph$), Medium and High speed ($10kph\sim$). The parameter update was not conducted in the zero-speed part.

3.1. Artificial Steering Model for Medium and High speed

This section descries the artificial steering model at speeds above 10 kph. A Balachandran defines the artificial steering feel based on the dynamic model of the vehicle (Balachandran and Gerdes 2013). This paper was modeled on electric power steering system. However, various methods of controlling electric power steering have also been studied(Dannöhl, Müller et al. 2012). Therefore, even when analyzing the dynamics of electric power steering, the steering feel varies according to the motor control algorithm.

In this dissertation, an artificial steering model was constructed through an empirical method. A steering model that satisfies objective evaluation index such as returnability, on-center feel, linearity, effective torque stiffness and steering sensitivity was constructed using the linear regression method (Norman 1984, 13674-1: 2003) (Salaani, Heydinger et al. 2004).

The artificial steering model according to vehicle speed is classified into stiffness and damping as follows:

$$T_{a.med}(\theta_{sw},\dot{\theta}_{sw},v_x) = T_{stiffness}(\theta_{sw},v_x) + T_{damping}(\dot{\theta}_{sw},v_x) \qquad (3.1)$$

Where $T_{a.med}$ is the artificial steering model for medium and high speed; $T_{stiffness}$ is the artificial stiffness model; $T_{damping}$ is the artificial damping model; θ_{sw} is the steering angle; v_x is the longitudinal vehicle speed. Since the friction torque is also a function of angular velocity, in this dissertation, the friction torque is also generated through the damping model. The stiffness model consists of linear combination of predefined functions as follows:

$$T_{stiffness}(\theta_{sw}, v_x) = \sum_{i=1}^{20} a_i(v_x) f_i(\theta_{sw}) \qquad (3.2)$$

Where a_i which depends on v_x is the coefficient of the predefined functions; f_i is predefined functions as shown in equation 3.3.

$$f_i(x) = \left((|x|+1)^{\frac{i+20}{40}} - 1\right) \times sgn(x) \qquad (3.3)$$

Figure 3.1 shows the characteristics of predefined functions.

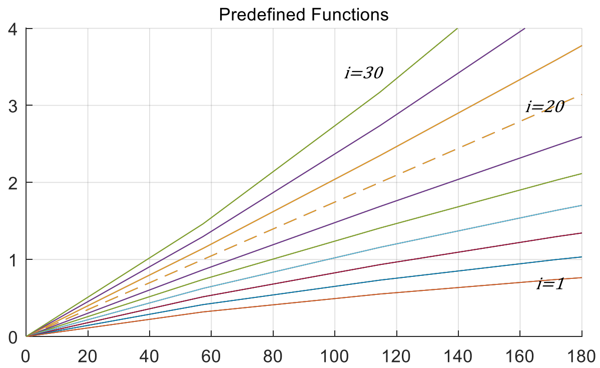

Figure 3.1 Predefined Functions

The damping model was also designed in the same method as the stiffness model as shown in equation 3.4.

$$T_{damping}(\dot{\theta}_{sw}, V) = \sum_{i=1}^{30} b_i(v_x) f_i(\dot{\theta}_{sw}) + b_{31}(v_x)\text{sat}\,(F_{sen}\dot{\theta}_{sw}) \qquad (3.4)$$

Where b_i which depends on v_x is also the coefficient of the predefined functions; F_{sen} is the sensitivity coefficient of friction model; $sat(.)$ means that saturation function that prevents the magnitude from exceeding 1. The predefined functions are determined by following rules. First, the derivative value at $x = 0$ is finite. If it is infinite like $f(x) = \sqrt{x}$, there is a difficulty in the passivity analysis in Chapter 5. The second is that the function value is 0 at $x = 0$. This is because the steering system has a stable point at 0deg and damping torque doesn't generate energy. Third, the stiffness model was used as concave function in the positive part because the tire lateral force is saturated as the tire slip angle increases. Lastly, the last term of the damping model is a term to express the friction torque, and a function whose gradient converges to zero is used. All functions that satisfy the above rules can be used as predefined functions. The more various predefined functions are, the easier it is to satisfies objective evaluation index.

a_i and b_i have been tuned to satisfies objective evaluation index. However, for the same reason as the predefined function design method, a_i and b_i are always positive. The objective evaluation index is defined based on the weave test and transition test.

The objective evaluation indices such as returnability, On-center Feel, Stiffness, Sensitivity and Linearity were converted into variables that are easy to tune. In this dissertation, the objective evaluation index shown in figure 3.2 was used.

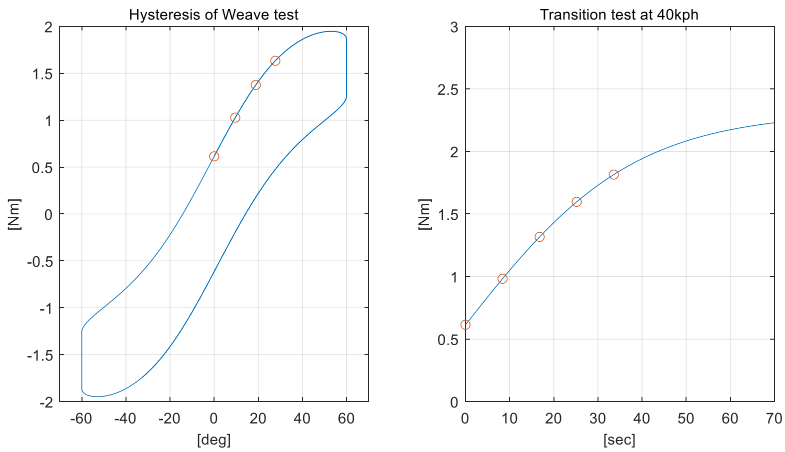

Figure 3.2 Objective evaluation index

In the weave test and transition test, the required torque was selected according to the position including 0deg. In the case of the weave test, the objective evaluation index was derived for two frequencies. Since there is also the load of the steering wheel system, the required torque was defined by excluding it. In order to satisfy the above requirements, the optimization problem as shown in equation 3.5 was solved.

$$\operatorname{argmin}_{a_i,b_i} \sum \left(T_{a.med}\left(\theta_{sw}, \dot{\theta}_{sw}, v_x\right) - T_{target}\right)^2$$

$$subject\ to\ a_i \geq 0\ , b_i \geq 0 \qquad (3.5)$$

Where T_{target} is the objective evaluation index. Interior point method was used to solve this optimization problem, which is the least square problem. Figure 3.3 is a graphical user interface designed to easily derive the objective evaluation index.

In the GUI, you can enter the conditions of each test such as angular velocity, slope of the transition test, amplitude and frequency of the weave test. You can also define the optimization problem by entering the target torque at each steering angle. When the optimization starts, the error result with the transition test and the weave test below are shown below. In addition, the designed artificial steering model and objective evaluation index are displayed at the top.

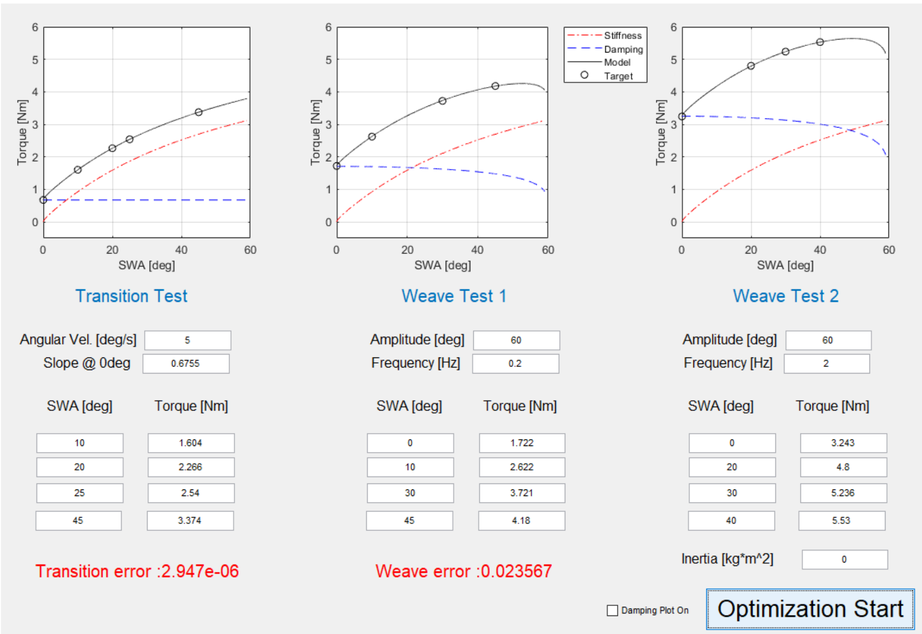

Figure 3.3 Graphical User Interface for Optimization

As a result, it is possible to derive a_i and b_i by performing optimization at a specific speed. In this dissertation, the above optimization was performed from 10kph to 140kph at 10kph intervals. a_i and b_i derived from a specific velocity were used as a continuous coefficient according to the velocity through interpolation as shown in equation 3.6.

$$a_i(V) = (1 - \frac{v_x}{10} + \left\lfloor\frac{v_x}{10}\right\rfloor)a_i\left(10\left\lfloor\frac{v_x}{10}\right\rfloor\right) + (\frac{v_x}{10} - \left\lfloor\frac{v_x}{10}\right\rfloor)a_i\left(10(\left\lfloor\frac{v_x}{10}\right\rfloor + 1)\right)$$

$$b_i(V) = (1 - \frac{v_x}{10} + \left\lfloor\frac{v_x}{10}\right\rfloor)b_i\left(10\left\lfloor\frac{v_x}{10}\right\rfloor\right) + (\frac{v_x}{10} - \left\lfloor\frac{v_x}{10}\right\rfloor)b_i\left(10(\left\lfloor\frac{v_x}{10}\right\rfloor + 1)\right)$$

$$where\ \lfloor x \rfloor\ is\ the\ integer\ part\ of\ x \qquad (3.6)$$

3.2. Artificial Steering Model for Zero speed

In this section, an artificial steering model for stopped situation where the vehicle is at zero speed is presented. Even at zero speed, the steering feel is determined by tire dynamics. However, it is impossible to use the artificial steering model designed in Chapter 3.1 because the dynamics of the tires are changed in the stopped situation (Bernard and Clover 1995). In the bicycle model, the longitudinal vehicle speed is in the denominator of the side slip angle term, so numerical problems can result when calculating the side slip angle at zero vehicle speed. Previously, this was not an issue as vehicle dynamics were designed based on when the vehicle is running.

In other words, it is impossible to design a tire model based on the slip angle using the bicycle model. Therefore, the steering system dynamics derived experimentally through the vehicle steering motion tests at zero vehicle speed are as follows:

$$T_{sw} = J_{sw}\ddot{\theta}_{sw} + b_{sw}\dot{\theta}_{sw} + F_{sw}sgn(\dot{\theta}_{sw}) + T_{tire} \tag{3.7}$$

Where J_{sw}, b_{sw} and F_{sw} are the inertia, damping and friction coefficient of the steering system; T_{tire} is tire force at zero vehicle speed as follows:

$T_{tire} = k_{tire}(\theta_{sw} - \theta_0)$

$where$

$$\begin{cases} \dot{\theta}_0 = 0 & \cdots |\theta_{sw} - \theta_0| < \theta_{limit} \quad (3.8a) \\ \dot{\theta}_0 = k_0\left(\theta_{sw} - \theta_0 - |\theta_{limit} - \theta_0| sat\left(\dfrac{\theta_{sw} - \theta_0}{|\theta_{limit} - \theta_0|}\right)\right) & \cdots |\theta_{sw} - \theta_0| \geq \theta_{limit} \quad (3.8b) \end{cases}$$

where θ_0 is the elastic equilibrium point; θ_{limit} is the elastic limit which is the distance between the steering angle and elastic equilibrium point; $sat(.)$ means that saturation function that prevents the magnitude from exceeding 1. k_{tire} is the stiffness coefficient at zero velocity; k_0 is the stiffness coefficient of elastic equilibrium point. T_{tire} does not directly mean the tire lateral force, but is a model of the load generated by the tire.

The equation 3.7 and equation 3.8 are the results obtained by reversely modeling through the steering system response that appears in the return situation after applying the steering input in the stop situation which is at zero speed. When the speed of the vehicle is not zero, the elastic equilibrium point θ_0 becomes zero, as shown in equation 3.8. This is explained through the phenomenon of returning to the on-center when the steering wheel is released after applying it while the vehicle is running. However, in a stopped situation, the steering wheel does not return to the on-center and stops halfway. This is a phenomenon that occurs because the tire dynamics in the stop situation is different from the driving situation. Therefore, an elastic equilibrium point θ_0 that is affected by the current steering wheel angle is introduced through experimental test.

When the vehicle is driving, the self-aligning torque acts as the on-center basis, and thus the steering wheel return to the on-center. When the vehicle is stopped, however, turning the steering wheel and releasing it does not return to the center and stops before it. This indicates that the elastic equilibrium point is not zero and is a variable affected by the applied steering input. Therefore, the elastic limit value θ_{limit} can be determined by how much the steering wheel has moved towards the center.

Figure.3.4 shows the return-to-center performance of the steering wheel at zero vehicle speed.

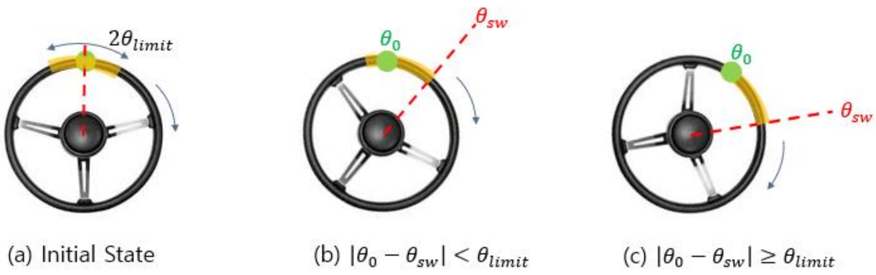

Figure 3.4 Steering characteristics at zero vhicle speed

In figure 3.4, the grean point is the elastic equilibrium point and the red point is the actual steering angle. The yellow range is the elastic limit. As the steering wheel is gradually turned from (a) to (b) and (c), the elastic equilibrium point moves according to the steering angle. Figure.3.5 is the result of releasing the steering wheel through actual vehicle experiment

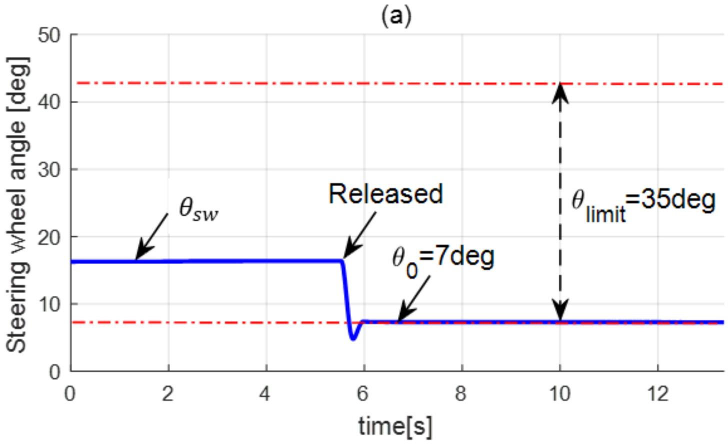

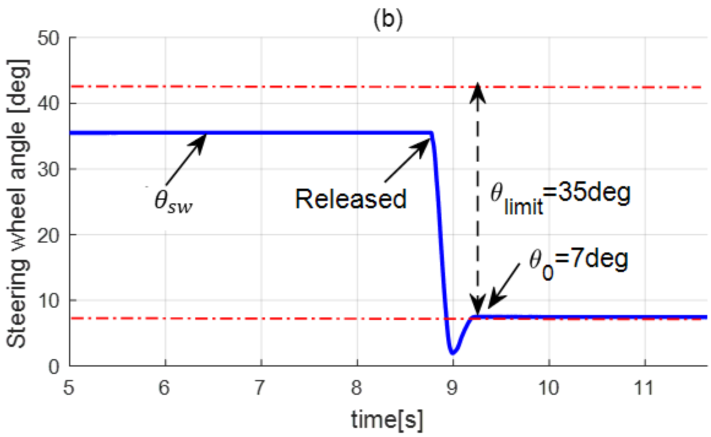

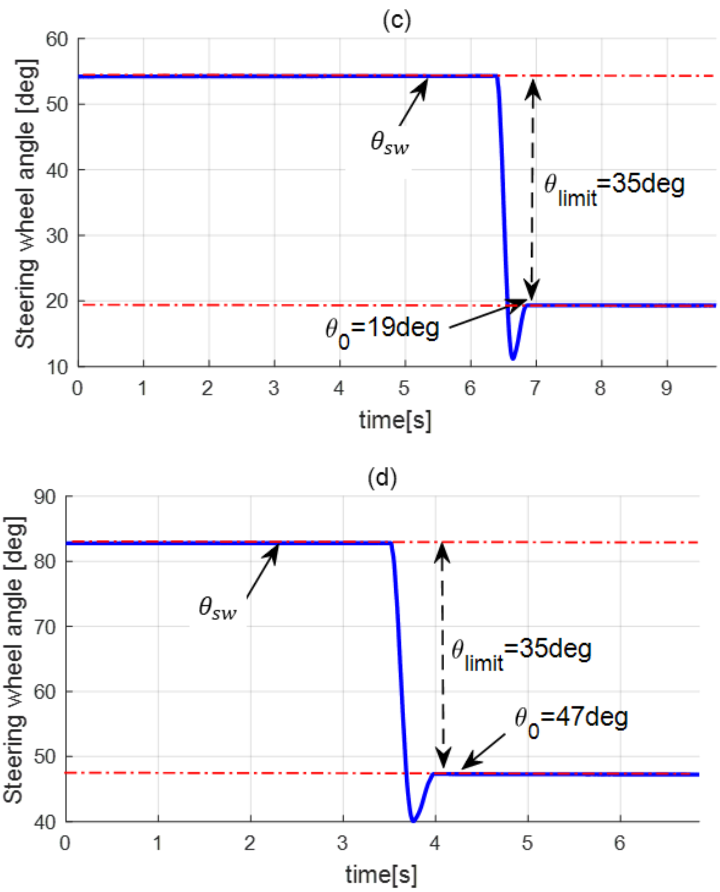

Figure 3.5 Vehicle test results when steering wheel is released

In the case of $|\theta_{sw} - \theta_0| < \theta_{limit}$ when the steering angle is released, it stops before it which is not the center, but the stop position is always constant. This means that the elastic equilibrium point θ_0 remains constant as shown in Figure.3.4(b). This can be confirmed from the actual vehicle test results in Figure.3.5(a) and Figure.3.5(b). If the steering input does not exceed the elastic limit, it always returns to the equilibrium point consistently no matter what moment the steering is released. In other words, the elastic equilibrium point θ_0 is remain constant. (=7deg)

However, when the steering wheel angle is gradually increases and satisfies the condition $|\theta_{sw} - \theta_0| \geq \theta_{limit}$, the elastic equilibrium point θ_0 changes as shown in Figure.3.4(c). This means that the larger the angle at which the steering angle is released, the larger the return position. Figure.3.5(c) and Figure.3.5(d) are experimental results showing the phenomenon shown in Figure.3.4(c). In Figure.3.5(c), when the steering angle is released, the condition $|\theta_{sw} - \theta_0| \geq \theta_{limit}$ is satisfied, and elastic equilibrium point value increases from 7 deg to 19 deg. Even if the steering wheel is released in a state larger than the steering angle in Figure.3.5(c), the elastic limit θ_{limit} value remains constant (=35 deg) and only the equilibrium point θ_0 increases. Figure.3.5(d) shows the results described above. In summary, the equation 3.8a reflects the Figure.3.5(a) and Figure.3.5(b) and the equation 3.8b shows the Figure.3.5(c) and Figure.3.5(d).

An artificial steering model for zero speed was designed based on the equation 3.7 experimentally derived through the vehicle steering motion test. It was designed by excluding inertia torque, which is difficult to estimate as follows:

$$T_{a.zero} = b_0\dot{\theta}_{sw} + F_0 sat(F_{sen}\dot{\theta}_{sw}) + T_{tire} \tag{3.7}$$

Where $T_{a.zero}$ is the artificial steering model for zero speed; b_0 and F_0 are the damping and friction coefficients of the artificial steering model. The sensitivity coefficient of damping model, F_{sen}, uses the same value as in equation 3.4. In the case of zero speed, unlike the driving situation, the objective evaluation index was not considered. Also, parameter update algorithm designed in Chapter 6.1 was not applied at zero speed. Instead, road disturbances such as curb collisions were reflected based on rack position tracking errors in Chapter 6.2.

3.3. Artificial Steering Model for Low Speed

This section describes the artificial steering model for low speed to design continuously between the model for zero speed and model for medium and high speed. The speed range covered in this section is from 0kph to 10kph. In vehicle experiments, when accelerating from a standstill, the equilibrium point moves to the origin. Therefore, while the speed changes from 0 to 10, the three parameters of the artificial steering model change: damping coefficient, stiffness coefficient, equilibrium point.

In the damping model, b_0 and F_0 defined in equation 3.7 must be matched with b_i in equation 3.4. Among the predefined models used in equation 3.4, the same function as the damping model used in equation 3.7 was used. Therefore, as shown in equation 3.8, a set of damping coefficients at zero speed are defined.

$$\begin{cases} b_{20}(0) = b_0 \\ b_{31}(0) = F_0 \\ b_i(0) = 0 \ \cdots i \neq 20,31 \end{cases} \qquad (3.8)$$

Linear interpolation of equation 3.6 can be used even between 0kph and 10kph through the set of damping coefficient at zero speed. In a similar method, the stiffness model was also designed as shown in equation 3.9.

$$\begin{cases} a_{20}(0) = k_{tire} \\ a_i(0) = 0 \ \cdots i \neq 20 \end{cases} \qquad (3.9)$$

Similarly, using the set of the stiffness coefficient at zero speed, an artificial steering model can be designed by interpolation. Lastly, the elastic equilibrium point was interpolated as follows:

$$\theta_0(V) = \left(1 - \frac{v_x}{10} + \left\lfloor \frac{v_x}{10} \right\rfloor\right) \theta_0(0) \qquad (3.10)$$

In summary, the artificial steering model for all speeds is as follows:

$$T_a\left(\theta_{sw}, \dot{\theta}_{sw}, v_x\right) = \sum_{i=1}^{30} b_i(v_x) f_i\left(\dot{\theta}_{sw}\right) + b_{31}(v_x)\,\mathrm{sat}\left(F_{sen}\dot{\theta}_{sw}\right) + \sum_{i=1}^{19} a_i(v_x) f_i(\theta_{sw}) + a_{20}(\theta_{sw} - \theta_0) \qquad (3.11)$$

Chapter 4 Parameter Estimation of Rack System Lateral Load Model.

This chapter describes the method for estimating road surface conditions through the rack system. The rack system is connected to the road wheel, which transmits road surface disturbance. Therefore, the current road surface conditions can be estimated indirectly through the rack system. The estimated road surface conditions are used to modify the artificial steering model through the parameter update algorithm. In this dissertation, the artificial steering model is modified by reflecting the road surface conditions of 10kph or more.

This chapter consists of three sections: Dynamic modeling of rack system, Rack position tracking control, Parameter estimation of rack system lateral load model. This dissertation analyzed the dynamics of the rack system and designed the estimation algorithm based on the Kalman filter. Motor torque and rack position are required as inputs to estimation algorithm. Rack position was measured through motor position sensor. Motor torque used motor control input without direct measurement. The motor control algorithm of the rack system is designed based on the reference paper.

4.1. Dynamic Modeling of Rack System

The rack system is connected to the road wheel, so tire load is transmitted. In this section, the rack system and the lateral load which is the tire force are modeled. Since the algorithm was designed on road surface conditions of 10kph or more, the tire model of zero speed such as equation 3.8 is not required. However, even though the tire force is different, since the rack system is the same structure, equation 3.7 can be applied equally. This section focuses on modeling the tire force above 10kph.

The tire model has been studied in various ways such as the linear tire model, magic formula of pacejka (Pacejka 2005), the brush model (Svendenius 2003) (Svendenius and Wittenmark 2003) and the physical model of Dugoff (Dugoff, Fancher et al. 1969). Figure 4.1 shows a comparison of tire models.

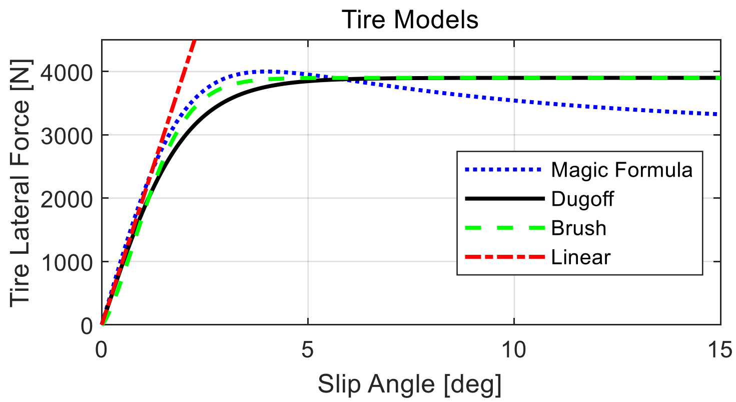

Figure 4.1 Comparison of tire models

In this dissertation, the linear tire model was used because it is more important to represent road surface information than the accuracy of the tire model. M kissai linearized the Dugoff model and used a tire model modeled as a linear region and a saturation region (Kissai, Monsuez et al. 2017). This linearized dugoff model has validated its utility in chassis control. Therefore, a linear tire model is sufficient to represent road surface conditions.

The linear tire model is as follows:

$$\begin{cases} F_{yf} = C_f \alpha_f = C_f (\delta_f - \dfrac{v_y + l_f \dot{\psi}}{v_x}) & (4.1a) \\ F_{yr} = C_r \alpha_r = C_r \left(- \dfrac{v_y - l_r \dot{\psi}}{v_x} \right) & (4.1b) \end{cases}$$

Where F_{yf} and F_{yr} are lateral tire force on front and rear wheel; C_f and C_r are the cornering stiffness of front and rear wheel; α_f and α_r are the side slip angle of front and rear wheel; v_x and v_y are longitudinal and lateral speed of the vehicle; l_f and l_r are distance between the front / rear axle and the center of gravity; δ_f is the front wheel angle; ψ is yaw angle.

The vehicle model was assumed to be a widely used bicycle model (Meijaard and Schwab 2006) as follows:

$$\begin{cases} \dot{v}_y = \dfrac{1}{m} \left(F_{yf} + F_{yr} \right) - v_x \gamma & (4.2a) \\ \dot{\gamma} = \dfrac{1}{I_z} \left(F_{yf} l_f + F_{yr} l_r \right) & (4.2b) \end{cases}$$

Where m and I_z are mass and inertia of the vehicle; $\gamma (= \dot{\psi})$ is yaw rate. The front lateral tire force can be derived by using the tire model of equation

4.1 and the bicycle model of equation 4.2. However, the calculation of the front lateral tire force is complex and does not need to be derived directly. The steady state is important because the reason for parameter estimation of the lateral load model is the change of road surface conditions. Transient response is not important because road surface conditions such as road friction coefficient change at low frequency. An algorithm that reflects high frequency disturbances such as gravel is shown in Chapter 6.2.

To derive the steady state of the lateral tire force, the steady state of the slip angle and yaw rate were derived from equation (4.1) and (4.2):

$$\begin{cases} \gamma_{ss} = \dfrac{1}{1 - \dfrac{m(l_f C_f - l_r C_r)}{2(l_r + l_f)^2 C_f C_r} v_x^2} \dfrac{v_x}{l_r + l_f} \delta_f \\ \beta_{ss} = \dfrac{1 - \dfrac{m l_f}{2 l l_r C_r} v_x^2}{1 - \dfrac{m(l_f C_f - l_r C_r)}{2(l_r + l_f)^2 C_f C_r} v_x^2} \dfrac{l_f}{(l_r + l_f)} \delta_f \end{cases} \tag{4.3}$$

Where β_{ss} and γ_{ss} are the steady state of slip angle. The steady state of lateral tire force obtained by substituting equation 4.3 for 4.1a as follows:

$$F_{y.ss} = C_f \left(\theta_f - \beta_{ss} - \frac{l_f \gamma_{ss}}{V_x} \right)$$

$$= \frac{mC_f C_r v_x^2}{2(l_r + l_f)^2 C_f C_r + m v_x^2 (l_r C_r - l_f C_f)} \delta_f \qquad (4.4)$$

Where $F_{y.ss}$ is the steady state of lateral tire force;

The lateral tire force generate moment in the tire. The equation for the moment applied to the tire is as follows:

$$M_{al} = F_{yf}(t_m + t_p) \qquad (4.5)$$

Where M_{al} is the aligning moment; t_m and t_p are mechanical trail and pneumatic trail. The mechanical trail depends on the caster angle and the pneumatic trail depends on the side slip angle (Hsu and Gerdes 2008). However, in this dissertation, to simplify the estimation model, they are used as a constant. The aligning moment is transmitted to the rack through the tie rod as follows:

$$F_{tie} = \frac{M_{al}}{l_{arm}} \qquad (4.6)$$

Where F_{tie} is tie rod force; l_{arm} is steering arm length. The tie rod and rack bar are connected by a ball joint. The relationship between tie rod force and rack force is as follows:

$$F_r = F_{tie} cos\phi \qquad (4.7)$$

Where F_r is rack force; ϕ is map of geometric relation between the tie rod and the rack bar as function of the rod displacement and the vertical wheel displacement. It was assumed that ϕ is a constant. Rack force is transmitted through the rack and pinion gear to the steering wheel.

Using equation 4.1 to 4.7, the dynamic equation for the rack system is organized as follows:

$$
\begin{aligned}
G_r T_{m.r} &= M_r \ddot{x}_r + b_r \dot{x}_r + F_r sgn(\dot{x}_r) + F_r \\
&= M_r \ddot{x}_r + b_r \dot{x}_r + F_r sgn(\dot{x}_r) + \frac{A_3 v_x^2}{A_1 + A_2 v_x^2} x_r \\
&= M_r \ddot{x}_r + b_r \dot{x}_r + F_r sgn(\dot{x}_r) + K_r x_r (4.8)
\end{aligned}
$$

Where M_r, b_r and F_r are mass, damping and friction coefficient of rack system; K_r is stiffness coefficient of lateral load model; x_r is rack position; $T_{m.r}$ is motor force of rack system; G_r is gear ratio between motor and rack bar; A_1, A_2 and A_3 are constant terms of lateral load model from equation 4.4 to 4.7. A_1, A_2 and A_3 were tuned based on vehicle test data. Motor torque and rack position were measured from vehicle test data of constant steering input. According to the speed, they were tuned as shown in Figure 4.2

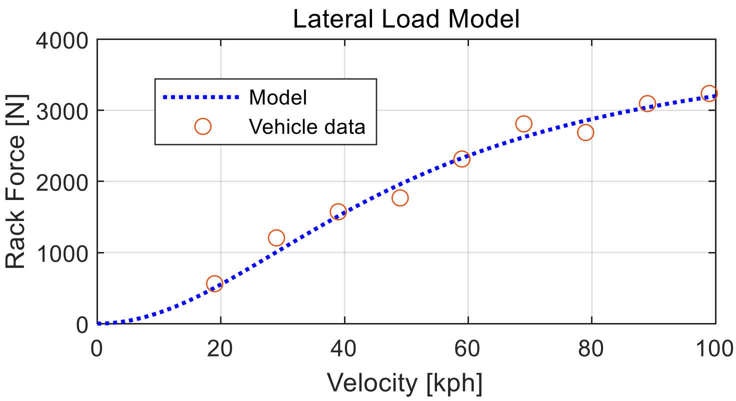

Figure 4.2 Vehicle Test Data with Constant Steering

4.2. Rack Position Tracking Control

To test steer-by-wire vehicles, rack position tracking control is required. In addition, the rack position tracking control algorithm is required for parameter estimation in equation 4.8. Kim K. proposed rack position tracking algorithm using adaptive sliding mode control(Kim, Lee et al. 2020). In this dissertation, the design process of the rack position tracking control algorithm is omitted.

The control torque input of the rack position tracking control algorithm is as follows:

$$T_{m.r} = M_r \ddot{x}_{r.d} + b_r \dot{x}_r + F_r sgn(\dot{x}_r) + \hat{k}_r x_r - \frac{x_r}{\lambda} \dot{e}_r - K sat(\frac{s}{\Phi}) \qquad (4.9)$$

Where x_d is desired rack position; $\hat{k}_r$ is equivalent stiffness which is adaptation parameter; λ is the time constant of the error dynamics; e_r is rack position tracking error. K is the positive sliding mode control gain; Φ is the positive tunable constant that controls the boundary layer of the sliding surface. The adaptation law of $\hat{k}_r$ is as follows:

$$\dot{\hat{k}}_r = -\frac{s \cdot x_r \cdot \lambda}{M_r \cdot \rho} \qquad (4.10)$$

Where s is sliding surface; ρ is the positive design value that determines the convergence speed of the parameter adaptation. Figure 4.3 shows the performance of rack position tracking control in normal driving condition.

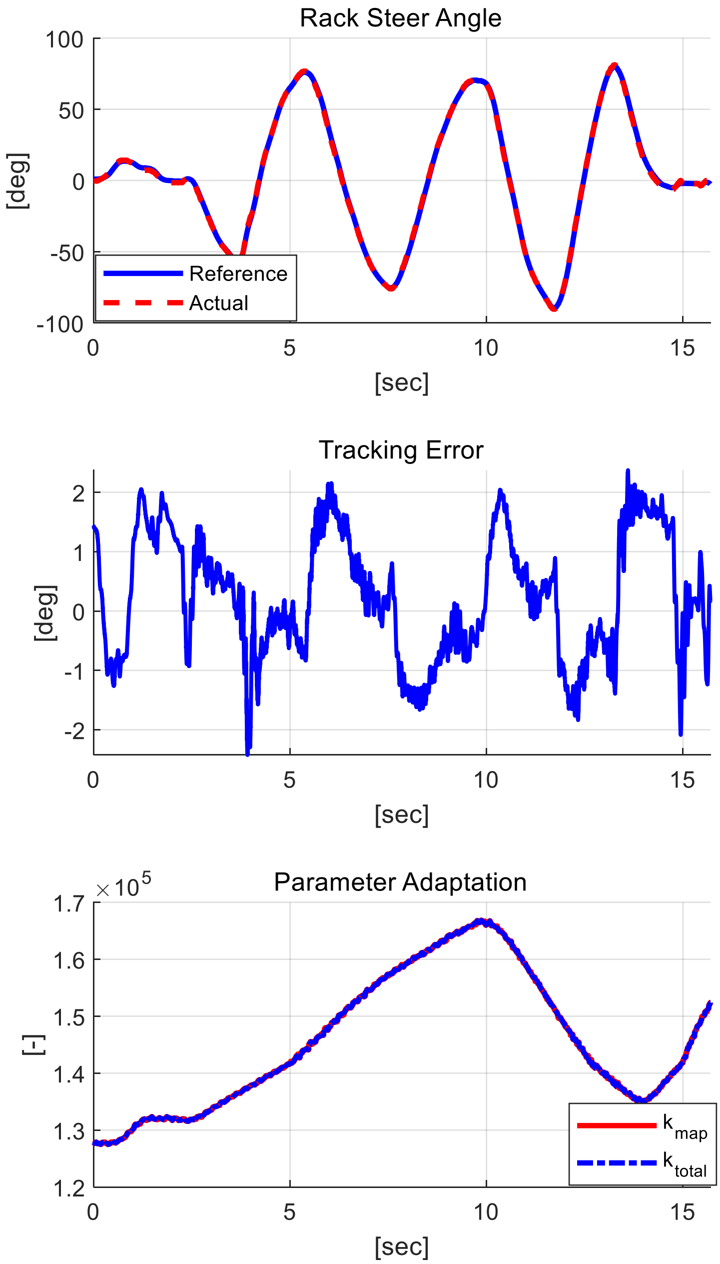

Rack Steer Angle
[deg]
100
50
0
-50
-100
Reference
Actual
0
5
10
15
[sec]
Tracking Error
[deg]
2
1
0
-1
-2
0
5
10
15
[sec]
Parameter Adaptation
×10^5
[-]
1.7
1.6
1.5
1.4
1.3
1.2
k_map
k_total
0
5
10
15
[sec]

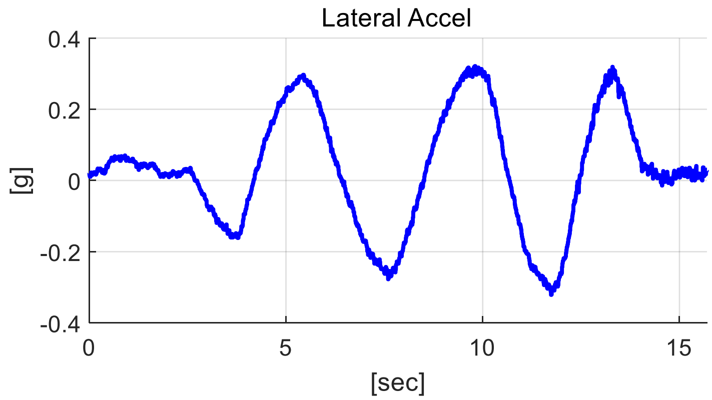

Figure 4.3 Performance of Rack Position Tracking Control in Normal Driving Condition

The rack position means the position of the rack bar and the rack steer means the position of the motor mounted to the rack bar. The rack steer is determined by converting the rack position considering the gear ratio (G_r). Figure 4.4 shows the performance of rack position tracking control in wet asphalt.

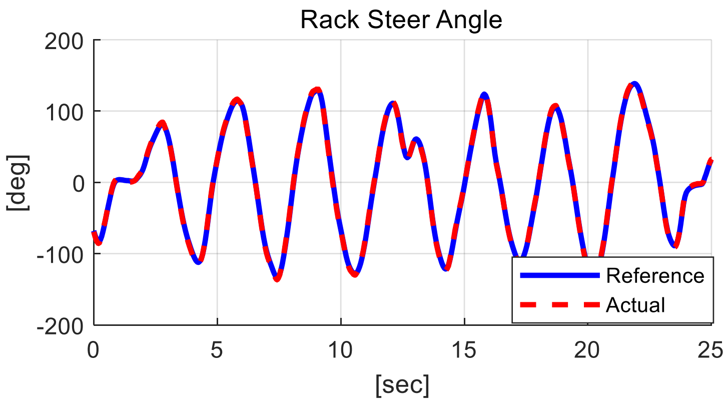

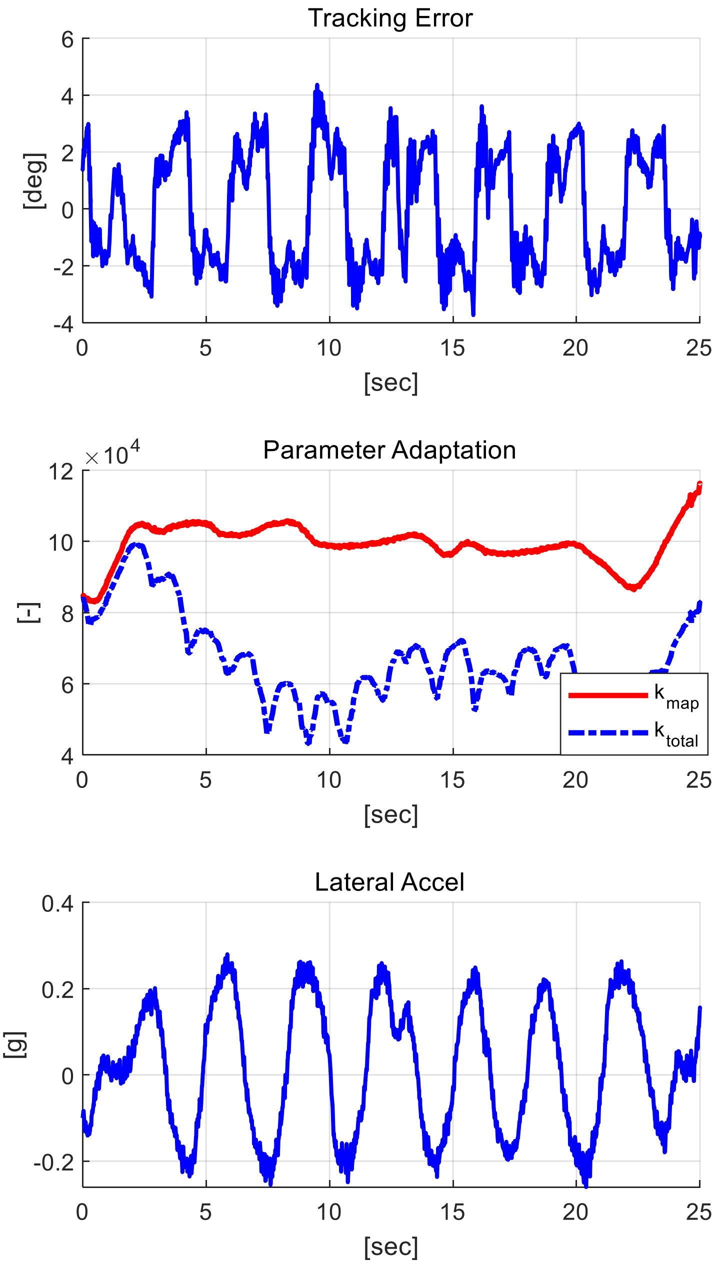

Figure 4.4 Performance of Rack Position Tracking Control in Normal Driving Condition

4.3. Parameter Estimation of Rack System Lateral Load Model

The parameter estimation of rack system lateral load model was conducted based on equation 4.8. There are second derivative and first derivative in equation 4.8, but only the rack position is measured through the motor position sensor of the steering motor as follows:

$$x_{sen}(t) = x_{sen}[h] = \Delta_{\mathrm{r}}\left(\left\lfloor \frac{x_r(hT)}{\Delta_{\mathrm{r}}} + \frac{1}{2} \right\rfloor\right) \qquad \forall t \in [hT; (h+1)T] \qquad (4.11)$$

Where x_{sen} is the rack position measurement of the motor position sensor; Δ_r is the combined resolution of the encoder and D/A converter in rack system; h denotes the discrete time variable; T is the sampling time of motor position sensor. Figure 4.4 shows the simulation result of the motor position sensor and the actual rack steer with 0.1deg resolution. Figure 4.4a is the result of weave test with 5deg magnitude, and Figure 4.4b shows an enlarged part of Figure 4.5a.

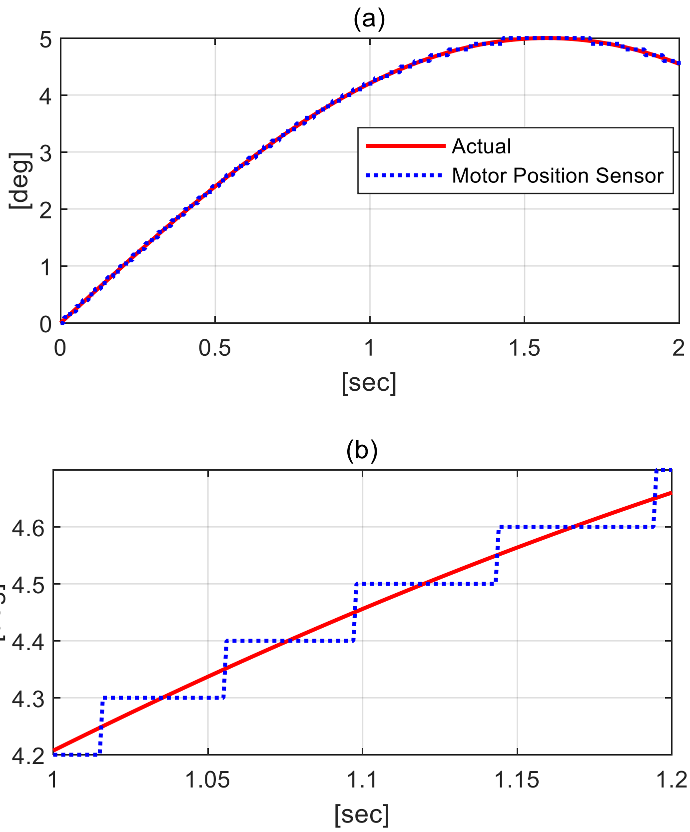

Figure 4.5 Simulation Result of Motor Position Sensor

The second derivative and first derivative were estimated based on the measured rack position using the finite difference method as follows:

$$\begin{cases} \hat{\dot{x}}_r[h] = \dfrac{x_{sen}[h] - x_{sen}[h-1]}{T} \\ \hat{\ddot{x}}_r[h] = \dfrac{\hat{\dot{x}}_r[h] - \hat{\dot{x}}_r[h-1]}{T} \end{cases} \qquad (4.12)$$

Where $\hat{\dot{x}}_r$ and $\hat{\ddot{x}}_r$ are the first and second derivative of rack position. The finite difference method has a small error when the sampling time and resolution are very small. However, Figure 4.6 shows that high frequency errors occur in the actual sensor environment.

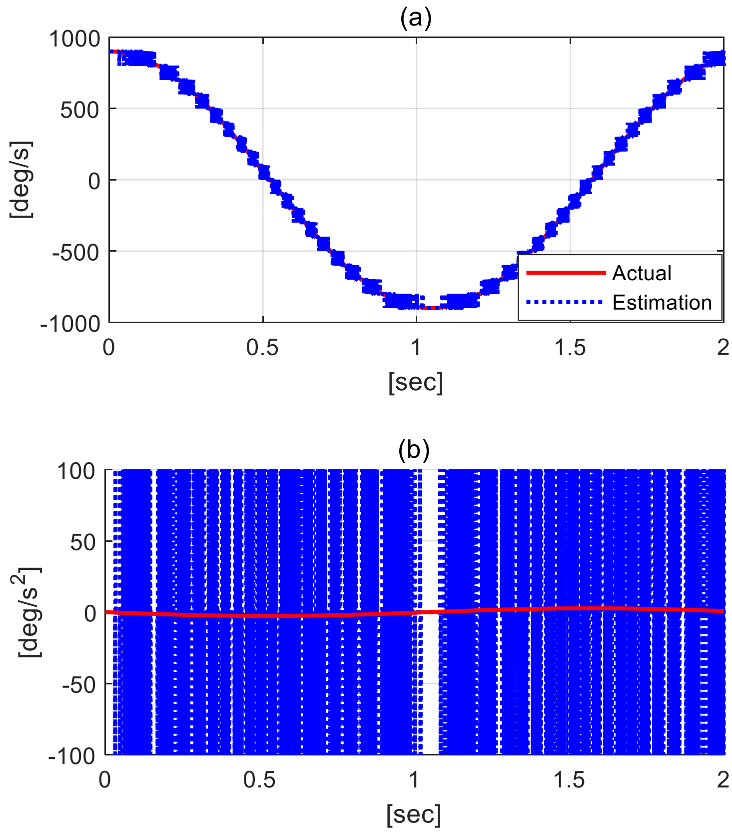

Figure 4.6 Estimation of Second and First Derivative

The angular velocity has a high frequency error and the angular acceleration is impossible to be used. Therefore, in parameter estimation, inertia is not used in Chapter 6.1. Using the estimated rack velocity and acceleration, the linear regression form is derived from equation 4.8 as follows:

$$G_r T_{m.r}[h] = M_r \hat{\ddot{x}}_r[h] + b_r \hat{\dot{x}}_r[h] + F_r sgn\left(\hat{\dot{x}}_r[h]\right) + K_r x_{sen}[h] + \Delta_e \quad (4.9)$$

Where Δ_e is the sum of the angular velocity estimation error and the lateral load model error. It is assumed that Δ_e is zero mean and white noise. M_r, b_r and F_r are unknown parameters and since the lateral load model includes cornering stiffness, it changes according to the road surface conditions. Therefore, the stiffness ratio was defined as follows:

$$\Delta_k = \frac{K_r}{\overline{K}_r} \quad (4.10)$$

Where $\overline{K}_r$ is the stiffness coefficient of lateral load model at nominal road condition which is dry asphalt. Since M_r, b_r, F_r and Δ_k are unknown, these variables are converted to vector form as follows:

$$\hat{X} = [\hat{M}_r \quad \hat{b}_r \quad \hat{F}_r \quad \hat{\Delta}_k]^T \quad (4.11)$$

Where $\hat{}$ means the estimated parameters. Using equation 4.11, the linear regression form of equation 4.9 is derived as follows:

$$Y[h] = G_r T_{m.r}[h]$$

$$H[h] = \left[\hat{\ddot{x}}_r[h] \quad \hat{\dot{x}}_r[h] \quad sgn\left(\hat{\dot{x}}_r[h]\right) \quad \overline{K}_r(v_x)\, x_{sen}[h]\right]^T \quad (4.12)$$

To estimate $\hat{X}$, a Kalman filter was used, equation 4.12 was used as a measurement model and a random walk model as shown in equation 4.13 was used as a process model(Spall and Wall 1984).

$$\dot{\hat{X}} = \Delta_p \qquad (4.13)$$

Where Δ_p is a process noise which is assumed to be zero mean and white noise. The process update equation and measurement update equation of the Kalman filter is as follows:

$$\hat{Y}[h] = H^T[h]\hat{X}[h-1]$$

$$\hat{X}[h] = \hat{X}[h-1] + K[h]\big(Y[h] - \hat{Y}[h]\big)$$

$$K[h] = \frac{P[h-1]H[h]}{R_2 + H^t[h]P[h-1]H[h]}$$

$$P[h] = P[h-1] + R_1 - \frac{P[h-1]H[h]H^T[h]P[h-1]}{R_2 + H^t[h]P[h-1]H[h]} \qquad (4.14)$$

Where $\hat{Y}$ is the prediction of measurement model, Y; K is the gain of measurement update; P is the estimated covariance matrix; R_1 is the covariance matrix of process noise, Δ_p; R_2 is the covariance of the measurement noise. Table 1 shows the values of design parameters used in Kalman filter.

Table 1 Design Parameter of Kalman Filter

Symbol	Value	Unit	Description
R_1	diag(R_m^2 , R_b^2 , R_f^2 , R_k^2)	[-]	The covariance matrix of process noise
R_m	2.7×10^{-7}	$kg \cdot m^2$	The square root of covariance of inertia
R_b	1.9×10^{-8}	$Nm/(rad/s)$	The square root of covariance of damping coefficient
R_f	3.5×10^{-9}	Nm	The square root of covariance of friction coefficient
R_k	5.2×10^{-5}	[-]	The square root of covariance of stiffness ratio
R_2	1	Nm^2	The square root of covariance of observation noise.

Chapter 5 Passivity Analysis of Haptic Control

This chapter focuses on passivity, one of the most important research areas in haptic control. In control system, passive component means that consumes but does not produce energy. The rack system to be rendered has a passive characteristic under normal driving conditions. Therefore, in conventional vehicles, there is no instable behavior or limit cycles. However, excessive haptic rendering can lead to instable behavior of limit cycles.

As shown in Figure 4.5 and Figure 4.6, the sampling rate and quantization of the sensor degrade the performance of the angular velocity and angular acceleration estimation. Using feedback control algorithm developed in the previous study under low sensor performance, it can become an active component due to the estimation error (Lee, Chang et al. 2017). Since the algorithm can make a limit cycle, the return-ability, which is the objective evaluation index, may be degraded. In this dissertation, a feedforward control algorithm that can be implemented at low sensor performance is designed. The detailed control algorithm is shown in Chapter 6. In Chapter 5, the passivity of the feedforward haptic control shown in equation 5.1 was analyzed.

$$T_{mot} = B_m\dot{\theta}_{sw} + F_m \cdot sgn(\dot{\theta}_{sw}) + K_m\theta_{sw} \qquad (5.1)$$

Where T_{mot} is motor torque which is control input; B_m, F_m and K_m is the damping, friction and stiffness coefficient of the rendering model. Each coefficient of the rendering model is determined by considering parameter estimation in Chapter 6. In Chapter 5, passivity conditions of the parameters of the rendering model are derived.

Energy analysis was conducted to derive the passivity conditions base on study about stability of haptic rendering (Diolaiti, Niemeyer et al. 2006). The rendering model consists of stiffness, damping and friction model. The passivity conditions were derived by analyzing the energy of each model in each section.

5.1. Energy Analysis

This section describes the analysis of the energy generated by the feedforward haptic control algorithm. Since the steering system was assumed to be a stiffness, damping, friction, and inertia model, when analyzing energy, the potential energy, kinetic energy, and dissipated energy were classified and analyzed. In addition, energy generated by haptic rendering error due to sensor performance was also analyzed.

Before energy analysis, the dynamics of the steering system to which haptic control is applied were derived as equation 2.2. The haptic control algorithm is the same as equation 5.1 but the angular velocity is estimated and used as in equation 4.12. The measurement of steering wheel angle and estimation of the steering wheel angular velocity is as follows:

$$\theta_{sen}(t) = \theta_{sen}[h] = \Delta_s \left(\left\lfloor \frac{\theta_{sw}(hT)}{\Delta_s} + \frac{1}{2} \right\rfloor \right) \qquad \forall t \in [hT; (h+1)T] \quad (5.1a)$$

$$\hat{\dot{\theta}}_{sw}[h] = \frac{\theta_{sen}[h] - \theta_{sen}[h-1]}{T} \qquad (5.2b)$$

Where θ_{sen} is the measurement of steering wheel angle; Δ_s is the resolution of steering angle sensor; $\hat{\dot{\theta}}_{sw}$ is the estimated steering wheel angular velocity.

In order to reduce excessive high frequency error, a low pass filter was designed. Using infinite impulse response filter, a low pass filter was designed as follows:

$$\dot{\theta}_{IIR}[h] = \gamma \dot{\theta}_{IIR}[h-1] + (1-\gamma)\hat{\dot{\theta}}_{sw}[h] \qquad (5.3)$$

Where $\dot{\theta}_{IIR}$ is the filtered steering wheel angular velocity; γ is a constant that is a coefficient of infinite impulse response filter. Using a filter in the estimator can increase the estimation error. However, it can be assumed that the range of angular acceleration is limited because there is a limit to the torque that the driver can apply and maximum steering angle is finite. In the limited angular acceleration range, the error of the angular velocity using the filter can be smaller. Figure 5.1 shows the angular velocity estimation performance using a low pass filter. Figure 5.1b shows an enlarged portion of figure 5.1a.

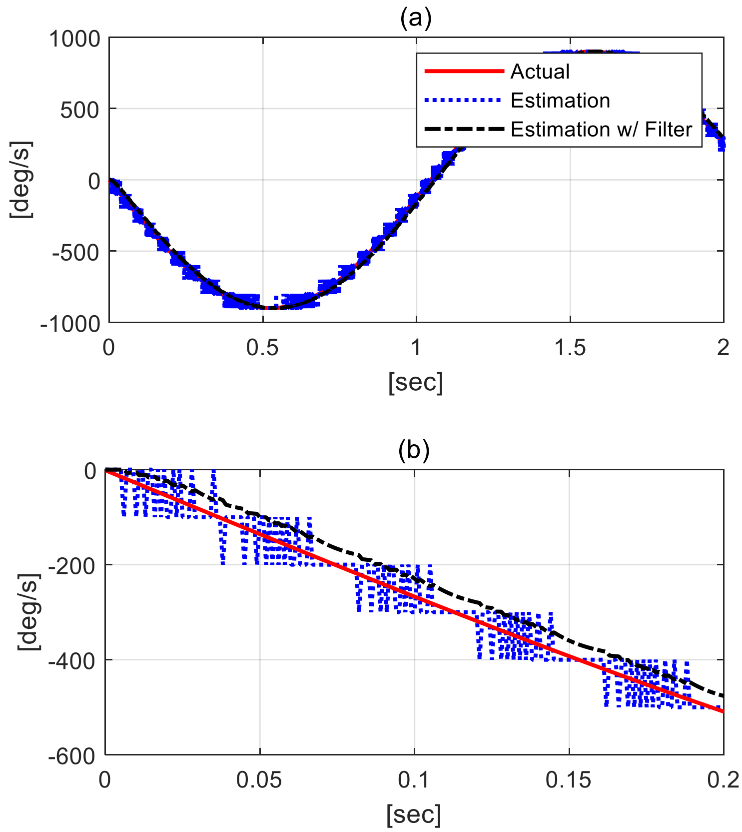

Figure 5.1 Estimation of Steering Angular Velocity with Low Pass Filter

Using measurable signals such as steering wheel angle, control algorithm of equation 5.1 is converted as follows:

$$T_{mot} = B_m\dot{\theta}_{IIR} + F_m \cdot sgn(\dot{\theta}_{IIR}) + K_m\theta_{sen} \qquad (5.4)$$

However, the sign function, a friction model, converts the estimation error to high frequency. Therefore, the friction model was assumed as the saturation function used previously as follows:

$$T_{friction} = F_m \cdot sat(k_f \cdot \dot{\theta}_{IIR})$$
$$= \begin{cases} F_m \cdot k_f \cdot \dot{\theta}_{IIR} & \cdots \left|\dot{\theta}_{IIR}\right| < 1/k_f \\ F_m \cdot sgn(\dot{\theta}_{IIR}) & \cdots else \end{cases} \qquad (5.5)$$

Where k_f is the saturation coefficient which determines sensitivity of friction model. If k_f converges to infinity, the equation 5.5 becomes the equation 5.4. It is assumed that equation 2.2, the dynamics of the steering system, is controlled by the equation 5.5. The driver was assumed to be a passive system except for the intended behavior. In energy analysis, a hands-off situation was assumed to minimize the driver's energy dissipation. The total energy in the steering system is as follows:

$$\int \Big(J_s\ddot{\theta}_{sw} + B_s\dot{\theta}_{sw} + F_s\,\mathrm{sgn}(\dot{\theta}_{sw}) + B_m\dot{\theta}_{IIR} + F_m \cdot sat(k_f \cdot \dot{\theta}_{IIR})$$
$$+ K_m\theta_{sen}\Big)\,\dot{\theta}_{sw}dt = 0 \qquad (5.6)$$

In equation 5.6, each term was classified as kinetic energy, potential energy, dissipated energy, and generated energy. The kinetic energy and potential energy that store energy are positive definite functions. The kinetic energy is as follows:

$$H_k = \int J_s \ddot{\theta}_{sw} \dot{\theta}_{sw} dt = \frac{1}{2} J_s \dot{\theta}_{sw}^2 \qquad (5.7)$$

Where H_k is the kinetic energy. Unlike kinetic energy, potential energy is not stored in a haptic device, but is virtually stored in a haptic control algorithm. To express the potential energy, the steering wheel angle which is continuous and quantized was defined as follows:

$$\theta_q = \Delta_s \left(\left\lfloor \frac{\theta_{sw}(t)}{\Delta_s} \right\rfloor + \frac{1}{2} \right) \qquad (5.8)$$

Where θ_q is the steering wheel angle which is continuous and quantized. Figure 5.2 shows a comparison of each steering wheel angle.

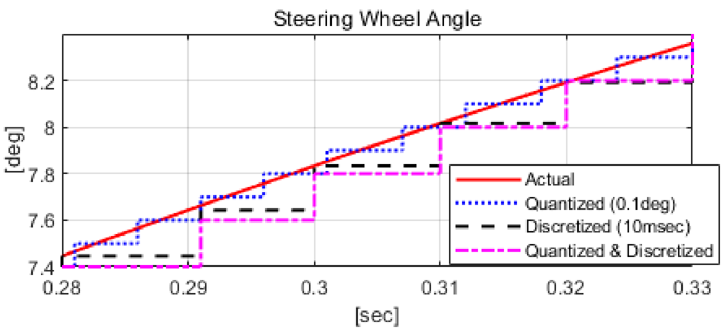

Figure 5.2 Comparison between Quantization and Discretization

When the potential energy is defined based on the quantized steering angle, the energy for a quantization error is added. The Quantization error is as follows:

$$\rho(x) = x - \lfloor x \rfloor \qquad (5.9)$$

Where ρ is a quantization error. The potential energy is as follows:

$$\begin{aligned}
H_p &= \int K_m \theta_q \dot{\theta}_{sw} dt = \int K_m \theta_q d\theta_{sw} \\
&= \int_0^{\Theta} K_m \Delta_s \left(\left\lfloor \frac{\theta_{sw}(t)}{\Delta_s} \right\rfloor + \frac{1}{2} \right) d\theta_{sw} \\
&= \int_0^{\Theta} K_m \left(\theta_{sw} - \Delta_s \rho\left(\frac{\theta_{sw}}{\Delta_s}\right) + \frac{1}{2}\Delta_s \right) d\theta_{sw} \\
&= \frac{1}{2} K_m\, \Theta^2 + \int_0^{\Theta} K_m \left(-\Delta_s \rho\left(\frac{\theta_{sw}}{\Delta_s}\right) + \frac{1}{2}\Delta_s \right) d\theta_{sw} \\
&= \frac{1}{2} K_m\, \Theta^2 + \frac{1}{2} K_m \Delta_s \Theta - \frac{1}{2} K_m \Delta_s^2 \left\lfloor \frac{\Theta}{\Delta_s} \right\rfloor - \frac{1}{2} K_m \Delta_s^2 \rho^2 \left(\frac{\Theta}{\Delta_s}\right) \\
&= \frac{1}{2} K_m\, \Theta^2 + \frac{1}{2} K_m \Delta_s^2 \left(\rho\left(\frac{\Theta}{\Delta_s}\right) - \rho^2 \left(\frac{\Theta}{\Delta_s}\right) \right) \qquad (5.10)
\end{aligned}$$

Where H_p is potential energy; When calculating energy, the initial value of steering angle was assumed to be 0. Θ is the final value of steering angle. In the process of equation 5.10, the following equation was used.

$$\int_0^{\chi} \rho(x) dx = \frac{1}{2} \lfloor \chi \rfloor + \frac{1}{2} \rho^2(\chi) \qquad (5.11)$$

Because $\rho\left(\frac{\Theta}{\Delta}\right)$ is between 0 and 1, it was proved that H_p is a positive definite function. Excluding the energies defined in equation 5.7 and 5.10, the remaining terms generate or dissipate energy. The stiffness energy is defined as follows:

$$E_s = \int K_m(\theta_{sen} - \theta_q)\dot{\theta}_{sw}dt \qquad (5.12)$$

Where E_s is the stiffness energy which can generate or dissipate energy. The damping and friction energy is defined as follows:

$$E_d = \int \left(B_s\dot{\theta}_{sw} + F_s \operatorname{sgn}(\dot{\theta}_{sw}) + B_m\dot{\theta}_{IIR} + F_m \cdot sat(k_f \cdot \dot{\theta}_{IIR})\right)\dot{\theta}_{sw}dt \qquad (5.13)$$

Where E_d is the damping and friction energy. Substituting the defined energies into equation 5.6 is as follows:

$$H_p + H_k + E_d + E_s = 0 \qquad (5.14)$$

Passivity means that the system always dissipate energy. If the following conditions are satisfied, the haptic device is a passive component.

$$E_d + E_s \geq 0 \qquad (5.15)$$

If the steering system is passive, unintended behavior and limit cycles do not occur. The stiffness energy was analyzed in section 5.2. The damping and friction energy were analyzed in section 5.3. In the last section, a range of rendering models that satisfies 5.15 was proposed based on the analyzed energy.

5.2. Stiffness Rendering

This section focuses on the analysis for stiffness energy, equation 5.11. Diolaiti has already conducted an analysis of stiffness energy (Diolaiti, Niemeyer et al. 2006). The stiffness energy was analyzed in the same method. In order to simplify the calculation, the energy analysis was performed at a time interval smaller than the sampling time. Equation 5.11 is converted as follows:

$$E_s(t, hT) = \int_{hT}^{t} K_m\big(\theta_{sen} - \theta_q\big)\dot{\theta}_{sw}dt \qquad (5.15)$$

Where h is integer; t is time which is satisfied $hT \le t < h(T+1)$. Using equation 5.1a and 5.8, stiffness energy is as follows:

$$E_s(t, hT) = \int_{hT}^{t} K_m\Delta_s(\left\lfloor\frac{\theta_{sw}(hT)}{\Delta_s}\right\rfloor - \left\lfloor\frac{\theta_{sw}(t)}{\Delta_s}\right\rfloor)\dot{\theta}_{sw}dt \qquad (5.16)$$

$$= \int_{hT}^{t} K_m\Delta_s(\frac{\theta_{sw}(hT)}{\Delta_s} - \frac{\theta_{sw}(t)}{\Delta_s} + \left\lfloor\frac{\theta_{sw}(hT)}{\Delta_s}\right\rfloor - \frac{\theta_{sw}(hT)}{\Delta_s} - \left\lfloor\frac{\theta_{sw}(t)}{\Delta_s}\right\rfloor + \frac{\theta_{sw}(t)}{\Delta_s})\dot{\theta}_{sw}dt$$

$$= \int_{hT}^{t} K_m\Delta_s\left(\frac{\theta_{sw}(hT)}{\Delta_s} - \frac{\theta_{sw}(t)}{\Delta_s} - \left(\rho\left(\frac{\theta_{sw}(hT)}{\Delta_s}\right) - \rho\left(\frac{\theta_{sw}(t)}{\Delta_s}\right)\right)\right)\dot{\theta}_{sw}dt$$

$\dot{\theta}_{sw}$ is the differential of the steering wheel angle by time, and terms excluding $\dot{\theta}_{sw}$ in equation 5.16 are terms for steering wheel angle. Therefore, equation 5.16 is as follows:

$$E_s(t,hT) = \int_{\theta_{sw}(hT)}^{\theta_{sw}(t)} K_m \Delta_s \left(\frac{\theta_{sw}(hT)}{\Delta_s} - \frac{\theta}{\Delta_s} + \rho\left(\frac{\theta}{\Delta_s}\right) - \rho\left(\frac{\theta_{sw}(hT)}{\Delta_s}\right) \right) d\theta \quad (5.17)$$

For convenience of calculation, equation 5.17 was calculated by dividing it into two parts. Each part is as follows:

$$\int_{\theta_{sw}(hT)}^{\theta_{sw}(t)} K_m \Delta_s \left(\frac{\theta_{sw}(hT)}{\Delta_s} - \frac{\theta}{\Delta_s} \right) d\theta = -\frac{1}{2} K_m \big(\theta_{sw}(hT) - \theta_{sw}(t)\big)^2$$

$$\begin{aligned}
&\int_{\theta_{sw}(hT)}^{\theta_{sw}(t)} K_m \Delta_s \left(\rho\left(\frac{\theta}{\Delta_s}\right) - \rho\left(\frac{\theta_{sw}(hT)}{\Delta_s}\right) \right) d\theta \\
&= -K_m \Delta_s^2 \rho\left(\frac{\theta_{sw}(hT)}{\Delta_s}\right)\left(\frac{\theta_{sw}(t)}{\Delta_s} - \frac{\theta_{sw}(hT)}{\Delta_s}\right) \\
&\quad + \frac{1}{2} K_m \Delta_s^2 \left(\left\lfloor \frac{\theta_{sw}(t)}{\Delta_s} \right\rfloor + \rho^2\left(\frac{\theta_{sw}(t)}{\Delta_s}\right) - \left\lfloor \frac{\theta_{sw}(hT)}{\Delta_s} \right\rfloor - \rho^2\left(\frac{\theta_{sw}(hT)}{\Delta_s}\right) \right) \\
&= K_m \Delta_s^2 \left(\frac{1}{2} - \rho\left(\frac{\theta_{sw}(hT)}{\Delta_s}\right) \right) \left(\left\lfloor \frac{\theta_{sw}(t)}{\Delta_s} \right\rfloor - \left\lfloor \frac{\theta_{sw}(hT)}{\Delta_s} \right\rfloor \right) \\
&\quad + K_m \Delta_s^2 \left(\rho\left(\frac{\theta_{sw}(t)}{\Delta_s}\right) - \rho\left(\frac{\theta_{sw}(hT)}{\Delta_s}\right) \right)^2 \qquad (5.18)
\end{aligned}$$

Since ρ and integer part, $\lfloor\cdot\rfloor$, are independent, the stiffness energy is minimized under the following conditions.

$$\rho\left(\frac{\theta_{sw}(t)}{\Delta_s}\right) = \rho\left(\frac{\theta_{sw}(hT)}{\Delta_s}\right) = \frac{1}{2}\left(\operatorname{sgn}\left(\left\lfloor \frac{\theta_{sw}(t)}{\Delta_s} \right\rfloor - \left\lfloor \frac{\theta_{sw}(hT)}{\Delta_s} \right\rfloor \right) + 1 \right) \quad (5.19)$$

Therefore, the stiffness energy satisfies the following equation.

$$E_s(t,hT) \geq -\frac{1}{2}K_m\left(\theta_{sw}(hT)-\theta_{sw}(t)\right)^2 - \frac{1}{2}K_m\Delta_s|\theta_{sw}(hT)-\theta_{sw}(t)| \tag{5.20}$$

The condition for equality in equation 5.20 is equation 5.19. Equation 5.19 indicates that $\theta_{sw}(hT)$ and $\theta_{sw}(t)$ are integer multiples of resolution. If the stiffness energy is negative, it means that energy is generated by the stiffness model.

5.3. Damping and Friction Rendering

This section focuses on the analysis of the damping model and friction model. The steering wheel angular velocity used when designing the damping and friction model is calculated by the equation 5.2b and 5.3. Although infinite impulse response filter used in the damping model is not an optimal method, it was used for convenience of analysis. Therefore, research on designing the optimal damping model is a future work.

The damping and friction energy has two parts that dissipate and generate energy. The load of the steering system dissipates energy. Dissipation energy is as follows:

$$E_{d.d} = \int B_s \dot{\theta}_{sw}^2 dt + \int F_s sgn(\dot{\theta}_{sw})\dot{\theta}_{sw} dt \qquad (5.21)$$

Where $E_{d.d}$ is dissipation energy of damping model. The minimum of damping energy was derived using Cauchy-Schwarz Inequality and the minimum of friction energy was derived using Triangle Inequality for integrals. The minimum of dissipation energy between time t_2 and t_1 is as follows:

$$\begin{aligned} E_{d.d}(t_2, t_1) &\geq B_s \frac{\left(\int_{t_1}^{t_2} \dot{\theta}_{sw} dt\right)^2}{\left(\int_{t_1}^{t_2} 1 dt\right)} + \left| F_s \int_{t_1}^{t_2} \dot{\theta}_{sw} dt \right| \\ &\geq B_s \frac{\left(\theta_{sw}(t_2) - \theta_{sw}(t_1)\right)^2}{t_2 - t_1} + F_s \left|\theta_{sw}(t_2) - \theta_{sw}(t_1)\right| \qquad (5.22) \end{aligned}$$

The damping model using the estimated angular velocity also generates energy. The energy generated by the damping model as follows:

$$E_{d,g} = \int \left(B_m \dot{\theta}_{IIR} + F_m \cdot sat\left(k_f \cdot \dot{\theta}_{IIR}\right)\right) \dot{\theta}_{sw} dt \tag{5.23}$$

Where $E_{d,g}$ is generation energy of damping model. The energy analysis was conducted by substituting equation 5.3 into equation 5.23. For the convenience of calculation of equation 5.23, the damping coefficient and friction coefficient were analyzed by substituting one variable as follows:

$$E_{d.g}(t, hT) = \int_{hT}^{t} B_F \dot{\theta}_{IIR} \dot{\theta}_{sw} dt$$

$$B_F = \begin{cases} B_m + F_m k_f & (|\dot{\theta}_{IIR}| < 1/k_f) \\ B_m + \dfrac{F_m}{\dot{\theta}_{IIR}} & (|\dot{\theta}_{IIR}| \geq 1/k_f) \end{cases} \tag{5.24}$$

Where B_F is the equivalent damping coefficient of damping model. As in equation 5.15, the generation energy of damping model, equation 5.24, was analyzed with the time interval as $[hT, t]$ as follows:

$$E_{d.g}(t, hT) = \int_{hT}^{t} B_F\left(\gamma \dot{\theta}_{IIR}[h-1] + (1-\gamma)\dot{\theta}_{sen}[h]\right)\dot{\theta}_{sw} dt$$

$$= \int_{hT}^{t} B_F \Big((1-\gamma)\dot{\theta}_{sen}[h] + (1-\gamma)\gamma\dot{\theta}_{sen}[h-1] + (1-\gamma)\gamma^2\dot{\theta}_{sen}[h-2]$$

$$+ (1-\gamma)\gamma^3\dot{\theta}_{sen}[h-3] + \cdots\Big)\dot{\theta}_{sw} dt$$

$$= \int_{hT}^{t} B_F(1-\gamma)\big(\dot{\theta}_{sen}[h] + \gamma\dot{\theta}_{sen}[h-1] + \gamma^2\dot{\theta}_{sen}[h-2] + \cdots\big)\dot{\theta}_{sw}dt$$

$$= B_F(1-\gamma)\left(\sum_{n=0}^{n=\infty} \gamma^n \frac{\theta_{sen}[h-n] - \theta_{sen}[h-1-n]}{T}\right) \int_{hT}^{t} \dot{\theta}_{sw}dt$$

$$= B_F(1-\gamma)\big(\theta_{sw}(t) - \theta_{sw}(hT)\big)\left(\sum_{n=0}^{n=\infty} \gamma^n \frac{\theta_{sen}[h-n] - \theta_{sen}[h-1-n]}{T}\right)$$

$$= B_F(1-\gamma)\big(\theta_{sw}(t) - \theta_{sw}(hT)\big)$$

$$\left(\sum_{n=0}^{n=\infty} \gamma^n \frac{\Delta_s\left(\left\lfloor\frac{\theta_{sw}\big((h-n)T\big)}{\Delta_s}\right\rfloor + \frac{1}{2}\right) - \Delta_s\left(\left\lfloor\frac{\theta_{sw}\big((h-n-1)T\big)}{\Delta_s}\right\rfloor + \frac{1}{2}\right)}{T}\right)$$

$$= B_F(1-\gamma)\big(\theta_{sw}(t) - \theta_{sw}(hT)\big)$$

$$\left(\sum_{n=0}^{n=\infty} \gamma^n \frac{\theta_{sw}\big((h-n)T\big) - \theta_{sw}\big((h-n-1)T\big)}{T}\right.$$

$$\left. - \Delta_s\left(\sum_{n=0}^{n=\infty} \gamma^n \frac{\left(\rho(\frac{\theta_{sw}(h-n)T)}{\Delta_s})\right) - \left(\rho(\frac{\theta_{sw}((h-n-1)T)}{\Delta_s})\right)}{T}\right)\right)$$

$$= B_F(1-\gamma)\big(\theta_{sw}(t) - \theta_{sw}(hT)\big)$$

$$\left(\begin{array}{c} \displaystyle\sum_{n=1}^{n=\infty} (1-\gamma)\gamma^{n-1} \frac{\theta_{sw}(hT) - \theta_{sw}\big((h-n)T\big)}{T} \\ \displaystyle -\frac{\Delta_s}{T}\left(\rho\left(\frac{\theta_{sw}(hT)}{\Delta_s}\right) - \sum_{n=1}^{n=\infty} (1-\gamma)\gamma^{n-1}\rho\left(\frac{\theta_{sw}\big((h-n)T\big)}{\Delta_s}\right)\right) \end{array}\right) \quad (5.25)$$

As in equation 5.19, $\rho\left(\frac{\theta_{sw}((h-n)T)}{\Delta_s}\right)$ is independent, so when the following equation is satisfied, the damping energy has a minimum value.

$$\begin{cases} \rho\left(\dfrac{\theta_{sw}(hT)}{\Delta_s}\right) = \dfrac{1 + sgn\big(\theta_{sw}(t) - \theta_{sw}(hT)\big)}{2} \\ \rho\left(\dfrac{\theta_{sw}\big((h-n)T\big)}{\Delta_s}\right) = \dfrac{1 - sgn\big(\theta_{sw}(t) - \theta_{sw}(hT)\big)}{2} \qquad n = 1,2,3\cdots \end{cases} \tag{5.26}$$

An inequality with equation 5.26 as the condition for equal sign is derived as follows:

$$E_{d.g}(t, hT)$$
$$\geq B_F(1-\gamma)^2\big(\theta_{sw}(t) - \theta_{sw}(hT)\big)\sum_{n=1}^{n=\infty}\gamma^{n-1}\frac{\theta_{sw}(hT) - \theta_{sw}\big((h-n)T\big)}{T}$$
$$-B_F(1-\gamma)\frac{\Delta_s}{T}|\theta_{sw}(t) - \theta_{sw}(hT)| \tag{5.27}$$

In addition, in order to obtain the minimum value of damping energy, the maximum and minimum of the steering wheel angular velocity and acceleration should be assumed. Assuming the range of the two variables is wide, it becomes a strict passive condition. To minimize passive energy, it is necessary to move as much as possible before time hT and in the opposite direction to the direction of movement after time hT. Since the calculation is difficult, a numerical solution was found and used. The energy term generated by the filter is defined as follows:

$$E_F = (1-\gamma)^2 \sum_{n=1}^{n=\infty} \gamma^{n-1} \frac{\theta_{sw}(hT) - \theta_{sw}\big((h-n)T\big)}{T} \tag{5.28}$$

Where E_F is energy term generated by the filter. Assuming the worst case in which the above energy can be generated, the value of E_F is shown in Figure 5.3

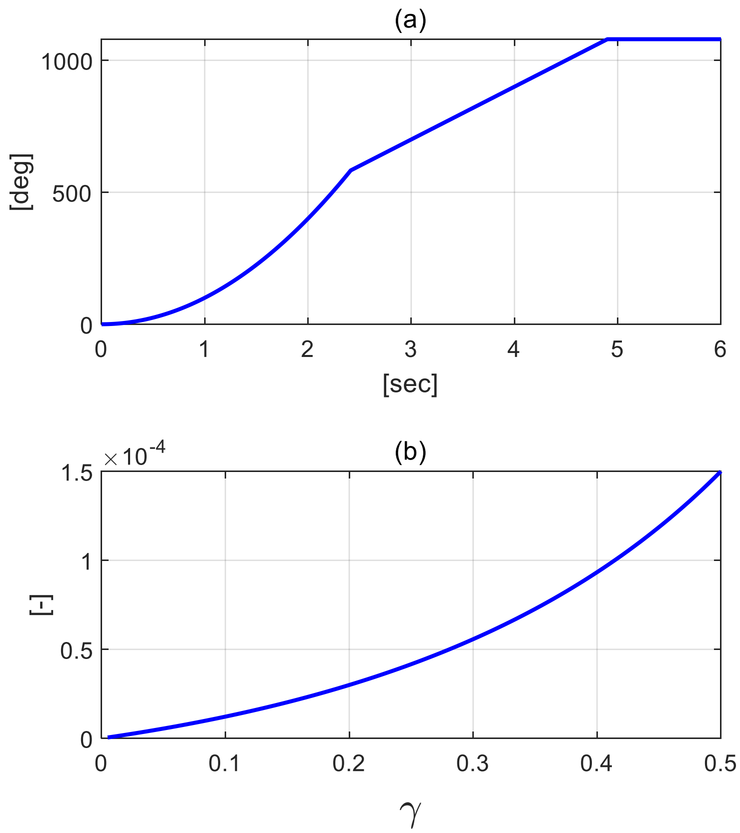

Figure 5.3 Energy Terms by Infinite Impulse Response Filter

Figure 5.3a is the angle difference that can occur in the worst case above, and figure 5.3b is the E_F value at that time. Therefore, the damping energy satisfies the following inequality equation:

$$
\begin{aligned}
&E_d(t, hT) \\
&\geq B_s \frac{\left(\theta_{sw}(t) - \theta_{sw}(hT)\right)^2}{t - hT} \\
&\quad \left(F_s - B_F\left(E_F(\gamma) + (1-\gamma)\frac{\Delta_s}{T}\right)\right)|\theta_{sw}(t) - \theta_{sw}(hT)| \qquad (5.29)
\end{aligned}
$$

If γ is 0, there is no filter, so energy is generated by quantization. As the γ increases, less energy is generated by quantization, but it can be seen that additional energy is generated due to filter error. When γ is too large, it diverges as shown in Figure 5.3, so it has been experimentally proven to use a value near 0.07.

5.4. Passivity Conditions

In the previous section, kinetic energy and damping energy were analyzed. This section derives passivity conditions based on equation 5.15. The kinetic energy, equation 5.20 and damping energy 5.29 are summed as follows:

$$
\begin{aligned}
E_s(t, hT) \geq & -\frac{1}{2} K_m \left(\theta_{sw}(hT) - \theta_{sw}(t)\right)^2 - \frac{1}{2} K_m \Delta_s |\theta_{sw}(hT) - \theta_{sw}(t)| \\
& + B_s \frac{\left(\theta_{sw}(t) - \theta_{sw}(hT)\right)^2}{t - hT} \\
& + \left(F_s - B_F \left(E_F(\gamma) + (1-\gamma) \frac{\Delta_s}{T}\right)\right) |\theta_{sw}(t) - \theta_{sw}(hT)|
\end{aligned}
\tag{5.30}
$$

If the minimum value of equation 5.30 is greater than 0, this system is always an energy consuming system. In other words, when the following conditions are satisfied, the passivity of the system is guaranteed.

$$
\begin{aligned}
& -\frac{1}{2} K_m \left(\theta_{sw}(hT) - \theta_{sw}(t)\right)^2 - \frac{1}{2} K_m \Delta_s |\theta_{sw}(hT) - \theta_{sw}(t)| \\
& + B_s \frac{\left(\theta_{sw}(t) - \theta_{sw}(hT)\right)^2}{t - hT} \\
& + \left(F_s - B_F \left(E_F(\gamma) + (1-\gamma) \frac{\Delta_s}{T}\right)\right) |\theta_{sw}(t) - \theta_{sw}(hT)| \geq 0
\end{aligned}
\tag{5.31}
$$

Dividing $|\theta_{sw}(t) - \theta_{sw}(hT)|$ by equation 5.31 and using the mean value theorem derives the following equation:

$$-\frac{\mathrm{T}}{2}K_m|\dot{\theta}_{sw}| - \frac{1}{2}K_m\Delta_s + B_s|\dot{\theta}_{sw}| + \left(F_s - B_F\left(E_F(\gamma) + (1-\gamma)\frac{\Delta_s}{T}\right)\right) \geq 0 \tag{5.32}$$

That necessary and sufficient conditions satisfied by equation 5.32 for all angular velocity are as follows:

$$-\frac{\mathrm{T}}{2}K_m + B_s \geq 0 \tag{5.33a}$$

$$-\frac{1}{2}K_m\Delta_s + \left(F_s - B_F\left(E_F(\gamma) + (1-\gamma)\frac{\Delta_s}{T}\right)\right) \geq 0 \tag{5.33b}$$

The equivalent damping defined in equation 5.24 for convenience of calculation was substituted into equation 5.33b as follows:

$$-\frac{1}{2}K_m\Delta_s + \left(F_s - (B_m + F_m k_f)\ \left(E_F(\gamma) + (1-\gamma)\frac{\Delta_s}{T}\right)\right) \geq 0 \tag{5.34a}$$

$$-\frac{1}{2}K_m\Delta_s + \left(F_s - \mathrm{F_m} - B_m\left(E_F(\gamma) + (1-\gamma)\frac{\Delta_s}{T}\right)\right) \geq 0 \tag{5.34b}$$

Since only one of equation 5.34a and 5.34b needs to be satisfied, it can be summarized as follows:

$$\min\left(-\frac{1}{2}K_m\Delta_s + \left(F_s - \left(B_m + F_m k_f\right)\left(E_F(\gamma) + (1-\gamma)\frac{\Delta_s}{T}\right)\right),\right.$$
$$\left.-\frac{1}{2}K_m\Delta_s + \left(F_s - \mathrm{F_m} - B_m\left(E_F(\gamma) + (1-\gamma)\frac{\Delta_s}{T}\right)\right)\right) \geq 0 \qquad (5.35)$$

In summary, when equation 5.33a and 5.35 are satisfied, the steering system is passive, so limit cycles and unstable behavior do not occur.

Chapter 6 Haptic Control Algorithm with Parameter Update

This chapter describes the feedforward impedance control and parameter update algorithm. The feedforward impedance control algorithm was designed based on the artificial steering model designed in Chapter 2. The artificial steering model was designed based on dry asphalt with a road surface friction of 0.85.

In section 6.1, a haptic control algorithm that generate the nominal steering feel in dry asphalt was proposed.

In section 6.2, a parameter update algorithm was proposed to reflect various road surface conditions. The road surface conditions were indirectly estimated by using parameter estimation for the lateral load model proposed in Chapter 4. The road surface condition mainly refers to a change in the coefficient of friction and is a change in the low frequency range. However, the parameters of the haptic control algorithm designed in section 6.1 should not always be changed according to the road surface condition. The parameters were updated based on the passivity conditions derived in Chapter 5 to prevent limit cycles or unstable behavior from occurring.

In section 6.3, a virtual spring model was introduced to reflect on high frequency disturbances such as curb impact.

6.1. Feedforward Impedance Control

Haptic control has been studied in not only the steering system, but also various haptic device. Niemeyer designed a haptic control algorithm by analyzing passivity in a teleoperation system (Niemeyer and Slotine 1991). The steering system is also a teleoperation system in which the steering wheel and rack are separated. However, since the rack system in a vehicle does not always have passive characteristics, there is no need to analyze passivity by integrating the two systems. In this dissertation, a haptic control without parameter update was designed using the artificial steering model designed in Chapter 3 and the steering wheel angular velocity estimation designed in Chapter 5 as a rendering target as follows:

$$
\begin{aligned}
&T_{f.o}\big(\theta_{sw}, \dot{\theta}_{sw}, v_x\big) \\
&= \sum_{i=1}^{30} b_i(v_x) f_i\big(\dot{\theta}_{IIR}\big) + b_{31}(v_x)\,\mathrm{sat}\big(F_{sen}\dot{\theta}_{IIR}\big) \\
&\qquad\qquad + \sum_{i=1}^{19} a_i(v_x) f_i(\theta_{sw}) + a_{20}(\theta_{sw} - \theta_0) \qquad (6.1)
\end{aligned}
$$

Where $T_{f.o}$ is feedforward impedance control without parameter update. Equation 3.11 can be distinguished by damping torque, friction torque and stiffness torque. The magnitude of each torque is determined through parameter update. The control algorithm considering parameter update is as follows:

$$
\begin{aligned}
&T_f(\theta_{sen}, \dot{\theta}_{IIR}, v_x) \\
&= \rho_d T_{f.d}(\dot{\theta}_{IIR}, v_x) + \rho_f T_{f.f}(\dot{\theta}_{IIR}, v_x) + \rho_k T_{f.s}(\theta_{sen}, v_x) \\
&= \rho_d \sum_{i=1}^{30} b_i(v_x) f_i(\dot{\theta}_{IIR}) + \rho_f b_{31}(v_x)\,\mathrm{sat}(F_{sen}\dot{\theta}_{IIR}) \\
&\qquad\qquad + \rho_k\Big(\sum_{i=1}^{19} a_i(v_x) f_i(\theta_{sen}) + a_{20}(\theta_{sen} - \theta_0)\Big) \qquad (6.2)
\end{aligned}
$$

Where T_f is feedforward impedance control with parameter update; $T_{f.d}$, $T_{f.f}$ and $T_{f.s}$ is the damping, friction and stiffness impedance control; ρ_d, ρ_f and ρ_k are the ratio coefficient of damping torque, friction torque and stiffness torque. In this dissertation, each coefficient is not updated below 10kph with different tire characteristics. Each coefficient is updated in a region of 10kph or more, which was assumed for the lateral load model in parameter estimation.

6.2. Parameter Update Algorithm

In this section, the coefficients defined in equation 6.2 are determined. The lateral load model could be estimated through parameter estimation designed in Chapter 4. The lateral load model is estimated with the state defined in equation 4.11. The damping coefficient, friction coefficient and stiffness ratio are used to update the parameter of the 6.2 equation as follows:

$$\begin{cases} \rho_d = \dfrac{\hat{b}_r}{\bar{b}_r} \\ \rho_f = \dfrac{\hat{F}_r}{\bar{F}_r} \\ \rho_k = \hat{\Delta}_k \end{cases} \qquad (6.3)$$

Where $\bar{b}_r$ and $\bar{F}_r$ are the nominal damping and friction coefficient of rack system with lateral load model. It is assumed that the parameters of equation 6.3 are less than 1 because it is a parameter estimation to consider the case of low friction coefficient such as wet and icy asphalt. However, if parameters are always updated based on equation 6.3, limit cycles or unstable behavior may occur. The parameter update rule was designed based on the passivity conditions of equation 5.33a and 5.35.

Since the artificial steering model is not a simple linear function, linearization is required. The vehicle targeted in this paper does not occur unstable behavior due to the limitation of motor power. Moreover, since all stiffness models have concave characteristics, the stiffness coefficient at the origin is the largest. Therefore, in this dissertation, passivity was determined based on the coefficients at the origin. In addition, the designed artificial steering model has the maximum damping and friction at 10kph, so this rendering model was analyzed for passivity at 10kph. Each coefficient at the origin becomes a coefficient of the rendering models in Chapter 5 as follows:

$$\begin{cases} B_m = \rho_d \left.\dfrac{\partial T_{f.d}}{\partial \dot{\theta}}\right|_{\dot{\theta}=0} \\ F_m = \rho_f \left.\dfrac{\partial T_{f.f}}{\partial \dot{\theta}}\right|_{\dot{\theta}=0} \\ K_m = \rho_k \left.\dfrac{\partial T_{f.k}}{\partial \theta}\right|_{\theta=0} \end{cases} \qquad (6.4)$$

However, the coefficient of infinite impulse response filter is also an important variable in passivity conditions. If the system becomes an active, the damping, friction to be rendered can be changed to make the system passive, but the coefficient of the infinite impulse response filter can be also changed. Figure 6.1 shows the maximum damping torque according to the filter coefficient.

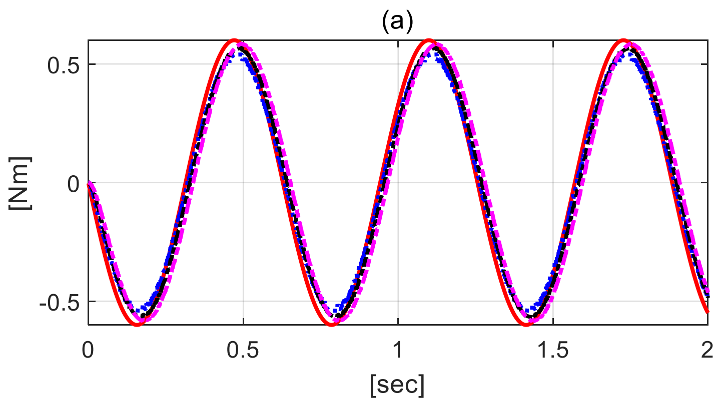

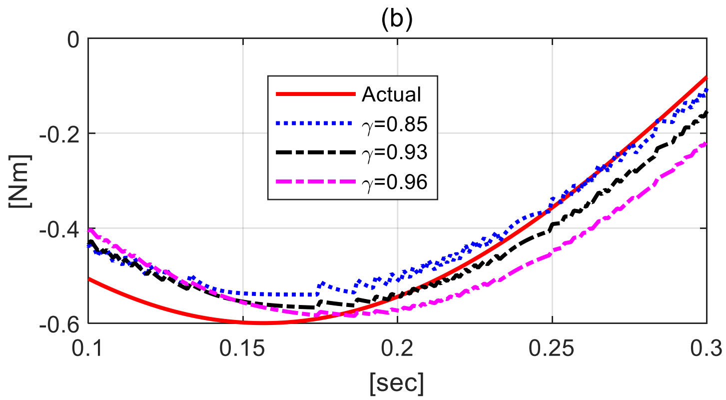

Figure 6.1 Maximum Damping Torque with Infinite Impulse Response Filter

In the figure above, different filter coefficients are used and all of them satisfy the passivity conditions, equation 5.33a and 5.35. The maximum damping coefficient is different depending on the gamma. If a filter coefficient that is too small is used, the acceptable damping coefficient is too small. On the other hand, as the filter coefficient increases, the delay of the damping torque increases. Also, a filter coefficient that is too large results in a smaller allowable damping coefficient.

N Colonnese defined the effective damping torque in haptic device (Colonnese, Sketch et al. 2014). Therefore, the damping coefficient and filter coefficient must be determined so that the effective damping torque can be maximized. The effective damping is defined as follows:

$$Eff.Damping = Re^{+}\{B_m \dot{\theta}_{IIR}(j\omega)\} \qquad (6.5)$$

The effective damping torque depends on the frequency of the input. The low frequency range is the artificial steering feel for which the objective evaluation index is defined, while the high frequency range is a bad feeling for the driver(Jiang, Deng et al. 2015). In addition, the most road environments mainly require low frequency angular velocity. Therefore, in this dissertation, effective damping was analyzed based on 0.2, 0.5, 1, and 2Hz. Using definition of the effective damping, equation 6.5, the effective damping to maximize is as follows:

$$\gamma_{op} = arg\max_{\gamma} \sum_{\frac{\omega}{2\pi}=0.2,0.5,1,2} Re^{+}\left\{B_m \dot{\theta}_{IIR}(j\omega)\right\}$$

$$subject\ to\ passivity\ conditions\ (equation\ 5.33a, 5.35) \qquad (6.5)$$

Where γ_{op} is the optimal filter coefficient. Equation 6.5 is an equation that derives the optimal filter coefficient (γ). It is hard to find the optimal solution in real time considering the passivity conditions. Therefore, the numerical solution was obtained from the following set of filter coefficient.

$$\gamma \in \left\{\gamma | \gamma = \frac{n}{100}, 85 \leq n \leq 95, n\ is\ natural\ number\right\} \qquad (6.6)$$

It is assumed that the artificial steering model designed in Chapter 3 is designed to always have a solution of equation 6.5 and 6.6 in the actual sensor performance. If the solution of equation 6.5 does not exist, the artificial steering feel cannot be stably rendered with the specification of the haptic device.

By determining and updating the optimal filter coefficient in real time, parameters can be updated while maintaining passivity. The parameter update algorithm can be summarized as follows:

Algorithm: Parameter Update Algorithm

Input: ρ_d, ρ_f, ρ_k, v_x

1. Compute coefficient of the rendering model

$$B_m(v_x) = \rho_d \frac{\partial T_{f.d}}{\partial \dot{\theta}}\bigg|_{\dot{\theta}=0}$$
$$F_m(v_x) = \rho_f \frac{\partial T_{f.f}}{\partial \dot{\theta}}\bigg|_{\dot{\theta}=0}$$
$$K_m(v_x) = \rho_k \frac{\partial T_{f.k}}{\partial \theta}\bigg|_{\theta=0}$$

2. for $\gamma \in \left\{\gamma | \gamma = \frac{n}{100}, 85 \leq n \leq 95, n\ is\ natural\ number\right\}$

2.1 Analyze the passivity conditions of the rendering model

$$\min\left(-\frac{1}{2}K_m\Delta_s + \left(F_s - \left(B_m + F_m k_f\right)\left(E_F(\gamma) + (1-\gamma)\frac{\Delta_s}{T}\right)\right),\right.$$
$$\left.-\frac{1}{2}K_m\Delta_s + \left(F_s - \mathrm{F_m} - B_m\left(E_F(\gamma) + (1-\gamma)\frac{\Delta_s}{T}\right)\right)\right) \geq 0$$

2.2 If rendering model is passive, compute effective damping

$$Eff.damping(\gamma) = \sum_{\frac{\omega}{2\pi}=0.2,0.5,1,2} Re^{+}\{B_m \dot{\theta}_{IIR}(j\omega)\}$$

3. Compute the arguments of the maxima

$$\gamma_{op} = arg\max_{\gamma} Eff.damping(\gamma)$$

4. Return γ_{op}

6.3. Virtual Spring Algorithm

In the previous section, the low frequency change of the road surface was stably reflected through parameter update. However, high frequency disturbance such as curb crashes and gravel roads must also be transmitted to the driver. The method of transmitting the force acting on the slave system such as the rack system to the master system has been studied a lot in the field of teleoperation

DA Lawrence analyzed the stability and transparency of the haptic control algorithm in bilateral teleoperation (Lawrence 1993). (Lawrence 1992). Transparency means transferring the impedance of the slave system through the master system. In the steering system, it can be called a master system called the steering wheel system and a slave system called the rack system. The algorithm for transparency is classified based on force and position. Among previous studies, a study on generating the steering feel based on rack force is a force-based algorithm. However, in this dissertation, if an algorithm is constructed based on rack force due to the limitation of sensor performance, a high frequency steering feel occurs. The comparative analysis is conducted in chapter 7. Instead, there is a way to use rack force indirectly. This is a method of transmitting the steering feel by utilizing the estimation error of the parameter estimator of the lateral load model designed in Chapter 4. The estimation error is as follows:

$$e_{rack\ force} = Y - \hat{Y} \qquad (6.7)$$

However, the estimation error is large scale because the algorithm is designed to reflect the low frequency. Therefore, in this dissertation, a position-based algorithm was designed. Park proposed position-based feedback haptic control algorithm(Park and Khatib 2006). As shown in figure 6.2 this paper also introduced a virtual spring to design an additional torque algorithm.

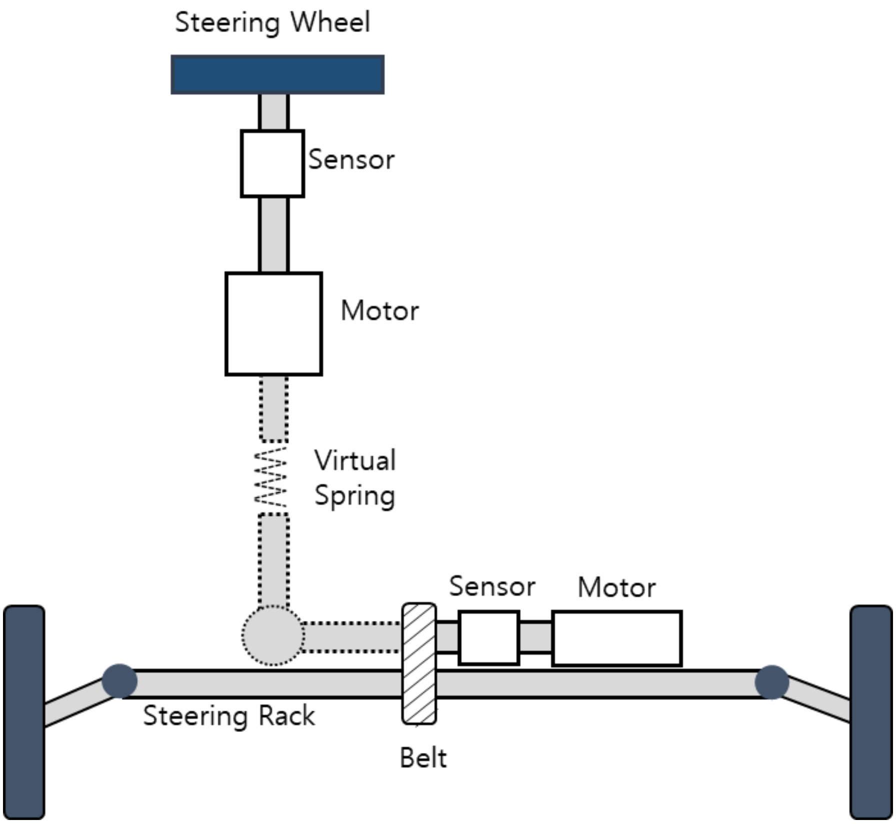

Figure 6.2 Cofiguration of steer-by-wire system with virtual spring

The haptic control algorithm added by virtual spring is as follows:

$$T_{add} = k_{virtual}(\theta_{sen}[h] - G_r x_r[h])$$
$$= k_{virtual}\left(\Delta_s\left(\left\lfloor\frac{\theta_{sw}(hT)}{\Delta_s} + \frac{1}{2}\right\rfloor\right) - G_r\Delta_r\left(\left\lfloor\frac{x_r(hT)}{\Delta_r} + \frac{1}{2}\right\rfloor\right)\right) \quad (6.7)$$

Where T_{add} is the additional haptic control input; $k_{virtual}$ is the stiffness coefficient of the virtual spring. However, equation 6.7 is the sensor performance and there is always a difference from the actual states. In addition, even though the rack position tracking algorithm in Chapter 4 is very robust, tracking errors always exist in nominal driving conditions. Therefore, a dead zone model was introduced to prevent this effect from being transmitted to the steering feel as follows:

$$T_{add.d}$$
$$= \begin{cases} k_{virtual}(\theta_{sen}[h] - G_r x_r[h] - \theta_z) & \theta_{sen}[h] - G_r x_r[h] \geq \theta_z \\ k_{virtual}(\theta_{sen}[h] - G_r x_r[h] + \theta_z) & \theta_{sen}[h] - G_r x_r[h] \leq -\theta_z \\ 0 & else \end{cases} \quad (6.8)$$

Where $T_{add.d}$ is the additional haptic control input with dead zone model; θ_z is the start and end of dead zone model. When θ_z is large, errors caused by performance limitations of angle and position sensor do not affect the steering feel, but high frequency disturbances of low magnitude are not transmitted. Although there is a trade-off, the experiment was conducted with a larger θ_z to generate a stable steering feel.

Using the proposed virtual spring model, the lateral load in the high frequency domain can be reflected in the steering feel. In summary, the haptic control algorithm used in this dissertation is as follows:

$$T_{haptic} = T_f\left(\theta_{sen}, \dot{\theta}_{IIR}(\gamma), v_x\right) + T_{add.d} \qquad (6.9)$$

Chapter 7 Simulation Studies and Vehicle Test

7.1. Computer Simulation Results for Passivity Conditions

In this section, the passivity conditions derived in Chapter 5 was validated through computer simulation using Matlab/Simulink. The steering wheel system was modeled using equation 2.2. Table 2 shows the parameters of the simulation model.

Table 2 The parameters of the simulation model.

Symbol	Value	Unit	Description
J_s	0.0019	$kg \cdot m^2$	The inertia coefficient of steering system
B_s	0.011	$Nm/(rad/s)$	The damping coefficient of steering system
F_s	0.25	Nm	The friction coefficient of steering system
T	0.001	sec	Sampling time
r	0.93	[-]	The coefficient of infinite impulse response filter
θ_{ini}	0.66	rad	Initial steering angle
Δ	0.1	deg	Resolution of angle sensor

There are five scenarios for validating passivity conditions: Stable rendering case, Unstable rendering case, 2 Unintended behavior case, Limit cycle case. To verify each scenario, a return test was conducted under the same conditions.

The first scenario is a stable rendering case, and a rendering model used in this scenario is as follows:

$$\begin{cases} B_m = 0.012 \\ K_m = 1.4 \\ F_m = 0.35 \\ k_f = 0.15 \\ \gamma = 0.93 \end{cases} \qquad (7.1)$$

The variables used in equation 7.1 satisfy the passivity conditions. Figure 7.1 shows the simulation results of the stable rendering case.

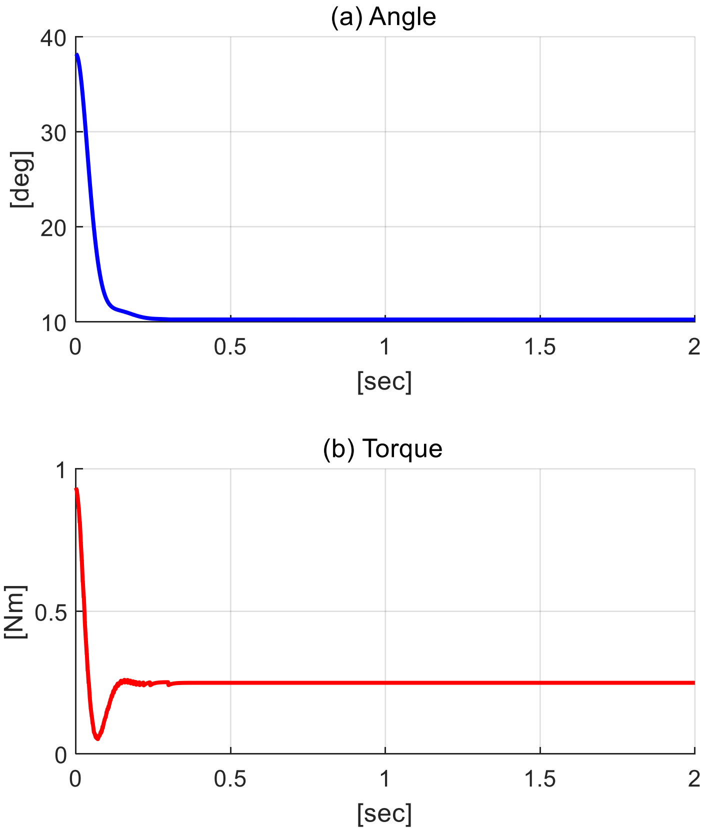

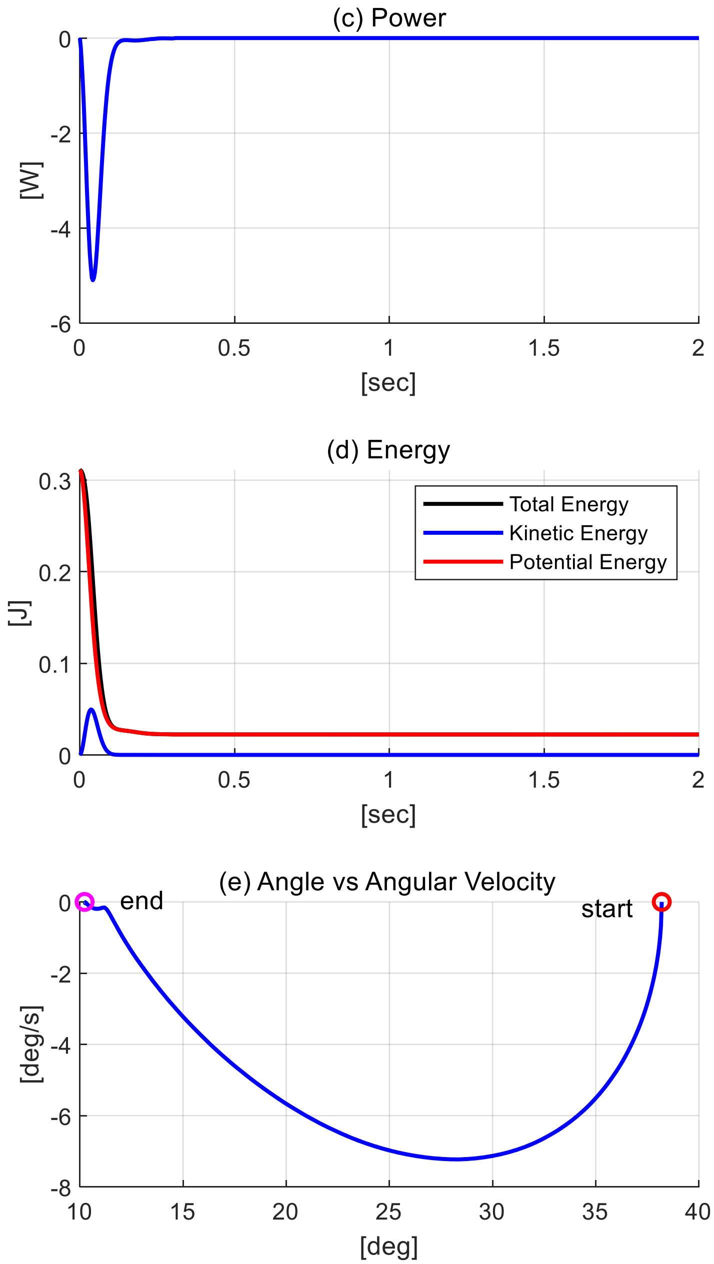

Figure 7.1 Simulation Result of Stable Rendering

In the stable rendering, simulation results show that steering wheel angle stops at 10deg and no energy is generated.

The second scenario is the unstable rendering case, and a rendering model used in this scenario is as follows:

$$\begin{cases} B_m = 0.005 \\ K_m = 33 \\ F_m = 0 \\ k_f = - \\ \gamma = 0.92 \end{cases} \qquad (7.2)$$

The variables used in equation 7.2 does not satisfied passivity conditions of equation 5.33a. Figure 7.2 shows the simulation results of the unstable rendering case.

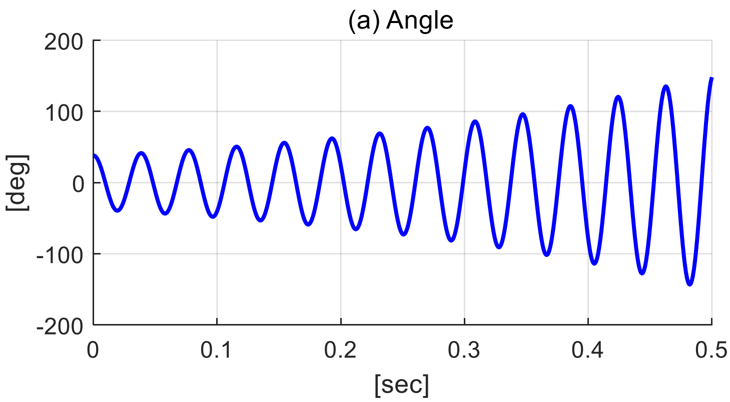

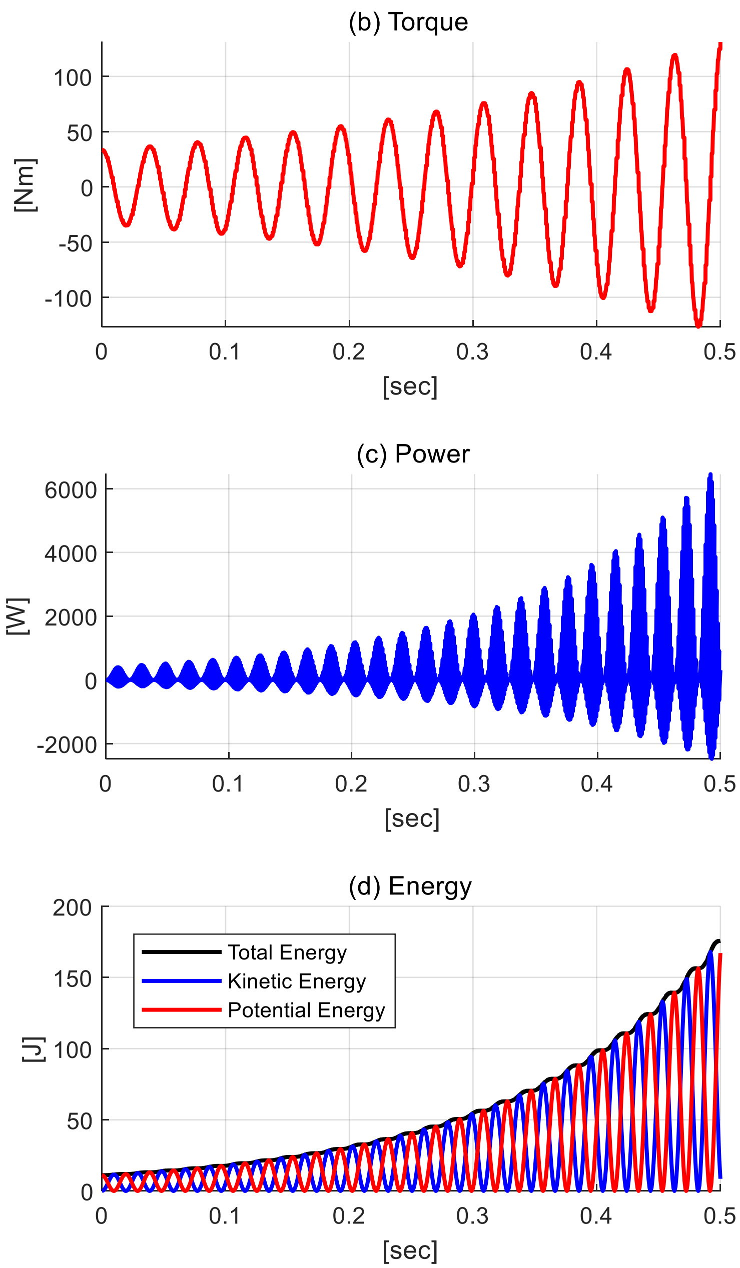
(b) Torque
[Nm]
100
50
0
-50
-100
0
0.1
0.2
0.3
0.4
0.5
[sec]
(c) Power
[W]
6000
4000
2000
0
-2000
0
0.1
0.2
0.3
0.4
0.5
[sec]
(d) Energy
[J]
200
150
100
50
0
Total Energy
Kinetic Energy
Potential Energy
0
0.1
0.2
0.3
0.4
0.5
[sec]

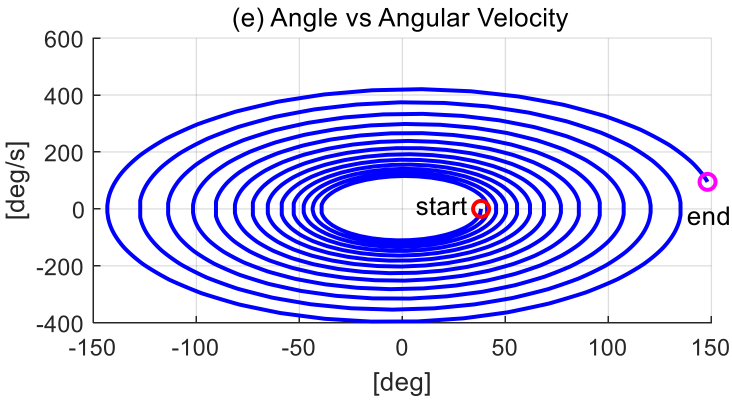

Figure 7.2 Simulation Result of Unstable Rendering

In the unstable rendering, simulation results show that steering wheel angle diverges and energy is generated.

The third scenario is the unintended behavior case, and a rendering model used in this scenario is as follows:

$$\begin{cases} B_m = 0.01 \\ K_m = 3 \\ F_m = 0.6 \\ k_f = 2 \\ \gamma = 0.96 \end{cases} \qquad (7.3)$$

The variables used in equation 7.3 does not satisfied passivity conditions of equation 5.35. Figure 7.3 shows the simulation results of the unintended behavior case.

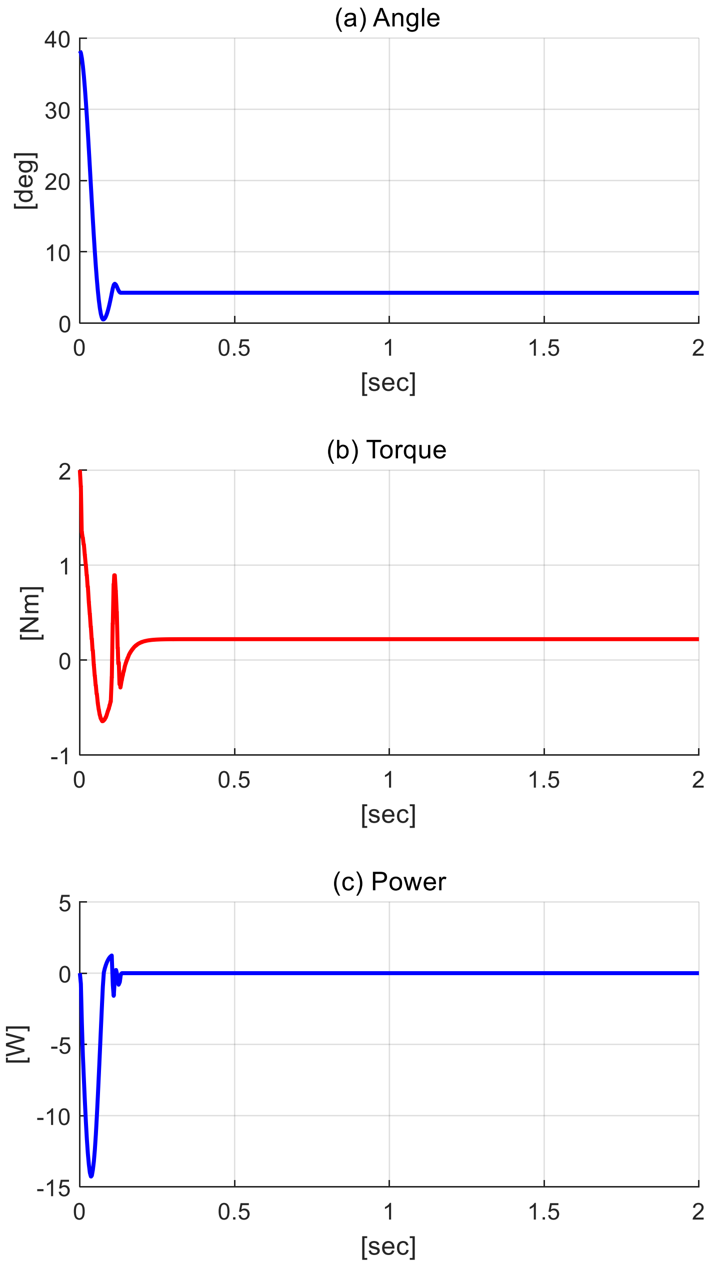

(a) Angle
[deg]
40
30
20
10
0
0
0.5
1
1.5
2
[sec]
(b) Torque
[Nm]
2
1
0
-1
0
0.5
1
1.5
2
[sec]
(c) Power
[W]
5
0
-5
-10
-15
0
0.5
1
1.5
2
[sec]

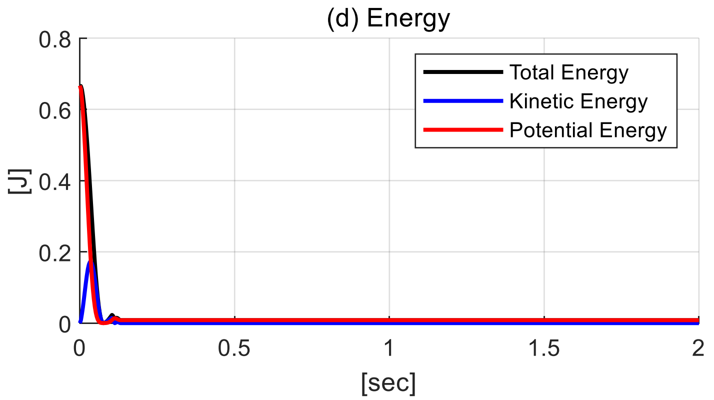

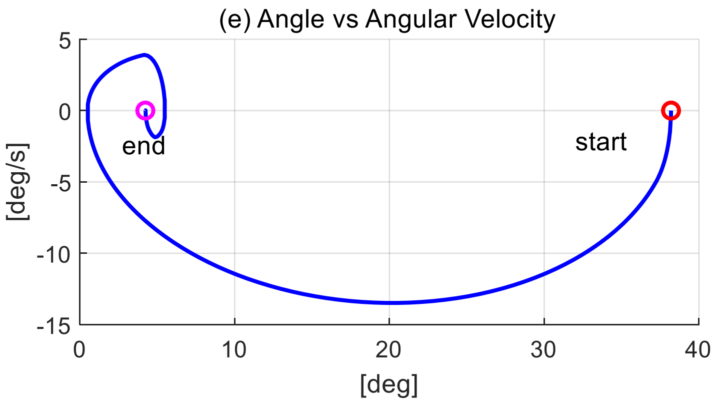

Figure 7.3 Simulation Result of Unintended Behavior 1

In the unintended behavior case, simulation results show that steering wheel moves differently from the passive system and energy is generated at some time. In addition, the origin is not 0deg. The fourth scenario is also the unintended behavior case. A rendering model used in this scenario is as follows:

$$\begin{cases} B_m = 0.01 \\ K_m = 1.5 \\ F_m = 0.6 \\ k_f = 3 \\ \gamma = 0.9 \end{cases} \qquad (7.4)$$

The variables used in equation 7.4 does not satisfied passivity conditions of equation 5.35. Figure 7.4 shows the simulation results of the unintended behavior case.

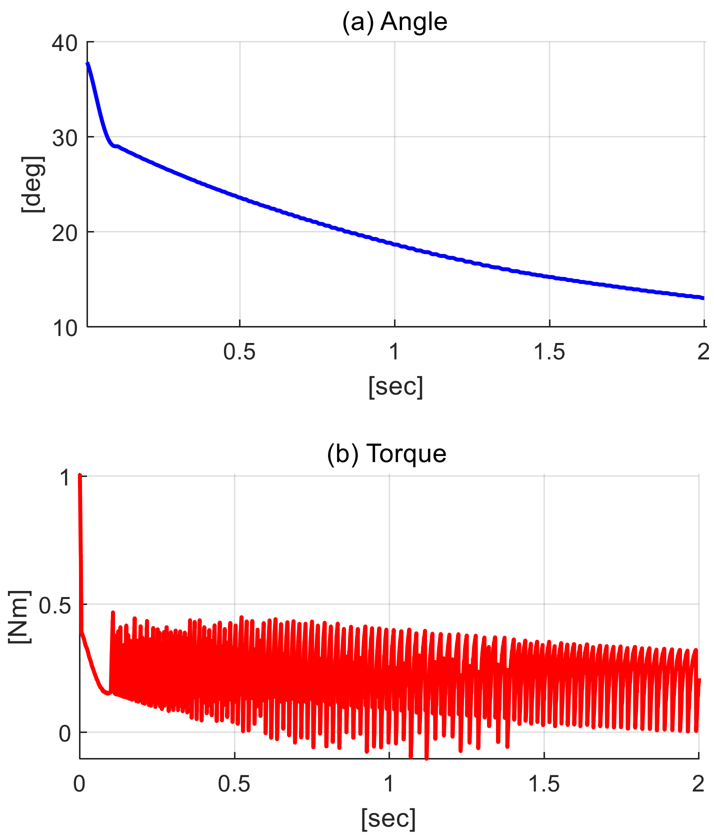

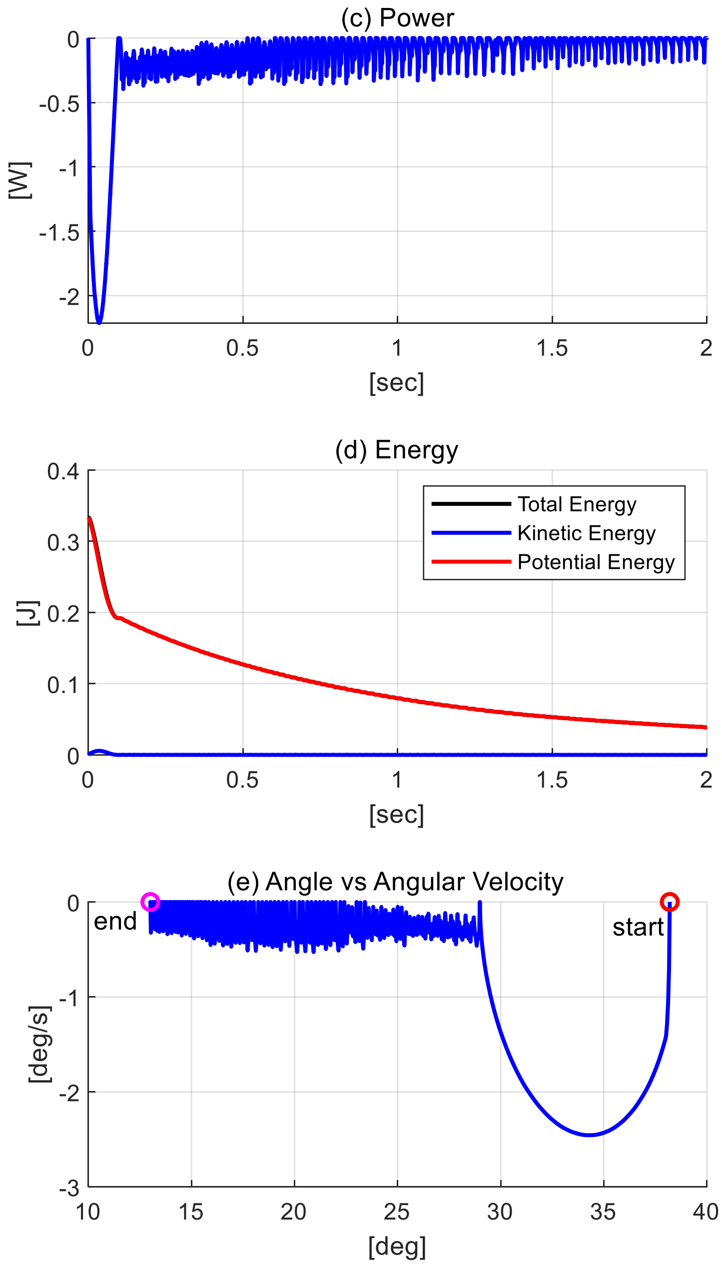

Figure 7.4 Simulation Result of Unintended Behavior 2

In another unintended behavior case, simulation results show that steering wheel moves also differently from the passive system and energy is generated at some time. In addition, the steering wheel moves and stops continuously. The last scenario is the limit cycle case. A rendering model used in this scenario is as follows:

$$\begin{cases} B_m = 0.01 \\ K_m = 3 \\ F_m = 0.6 \\ k_f = 200 \\ \gamma = 0.93 \end{cases} \qquad (7.5)$$

The variables used in equation 7.5 does not satisfied passivity conditions of equation 5.35. Figure 7.5 shows the simulation results of the unintended behavior case.

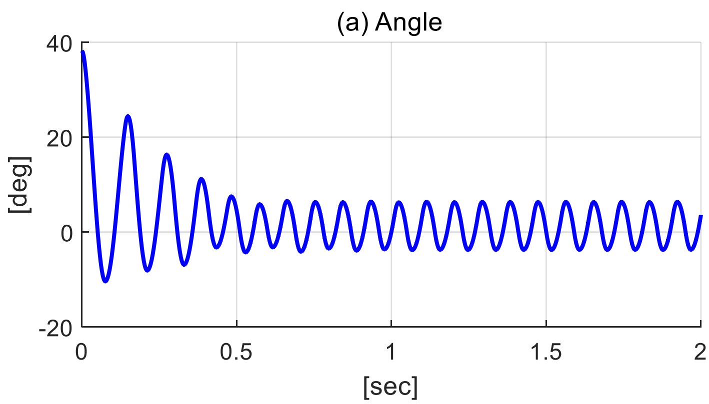

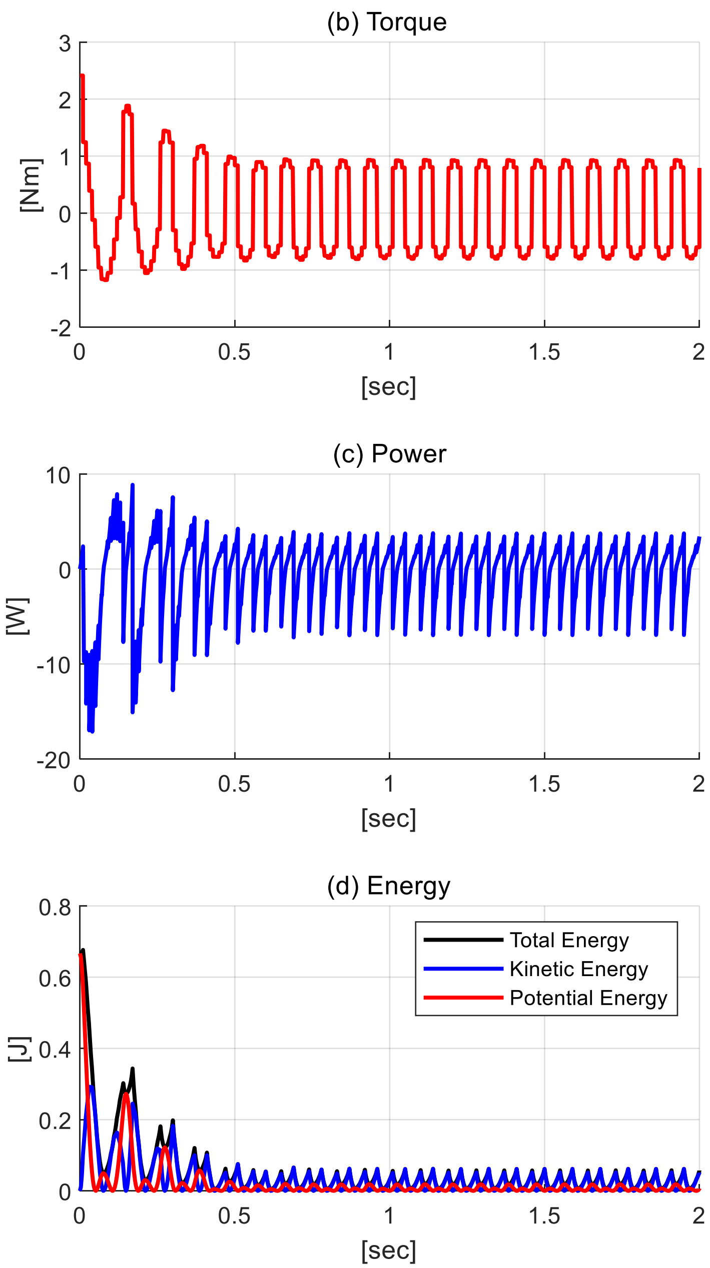
(b) Torque
[Nm]
[sec]
(c) Power
[W]
[sec]
(d) Energy
[J]
[sec]
Total Energy
Kinetic Energy
Potential Energy

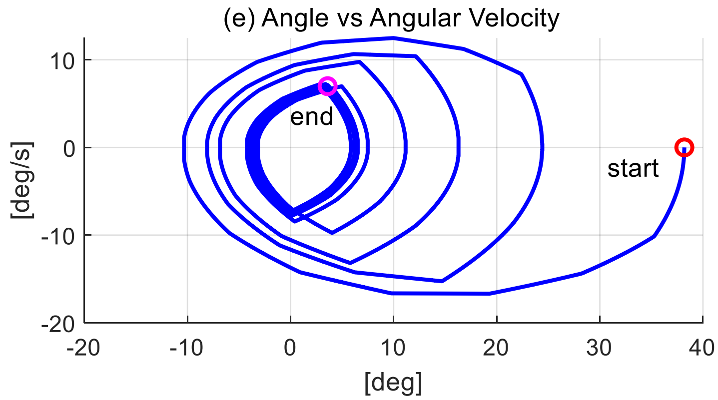

Figure 7.5 Simulation Result of Limit Cycle

In the limit cycle case, simulation results show that steering wheel moves continuously and energy is generated at some time. In addition, there is a limit cycle. Through these simulation result, passivity conditions are validated.

7.2. Computer Simulation Results for Haptic Control Algorithm

This section shows computer simulation results for haptic control algorithm. To evaluate the performance of haptic control algorithm, the evaluation index was introduced as shown in Figure 7.6 (박영대, 이병림 et al. 2019)

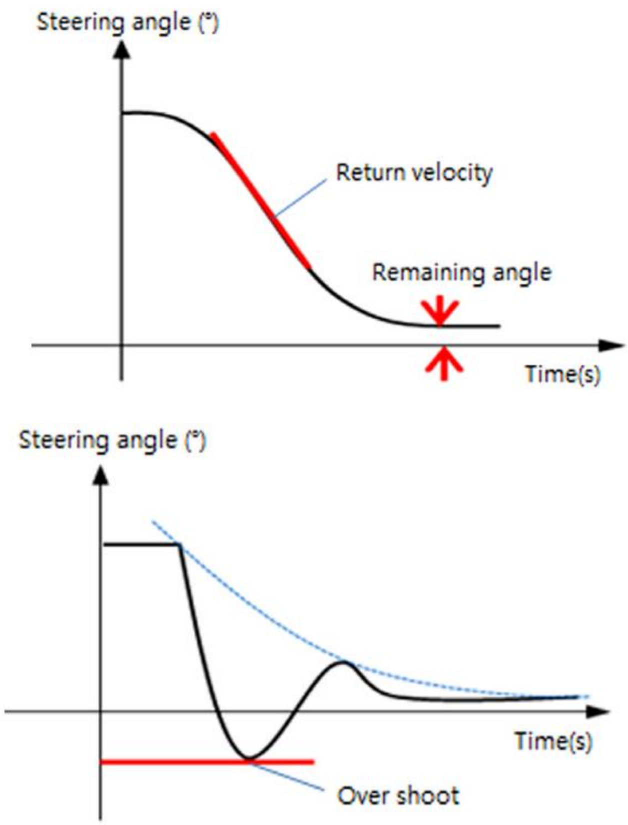

Figure 7.6 Evaluation Index in Return Test

In return test which is a hands-off simulation, the overshoot occurs and the angle remains in steady state. The overshoot and the remaining angle must be small for the haptic control algorithm to be stable. Figure 7.7 is the result of the return test in the target steering model. The return test was performed at 5 deg intervals from 60deg to 0deg.

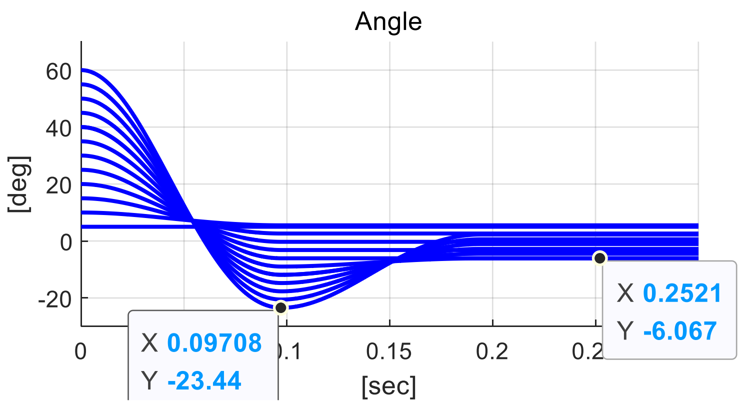

Figure 7.7 Return Test Result of Target Steering Model at 80kph

In the target model, the overshoot is 23.44deg and the maximum remaining angle is 6.067deg. The result of the return test of the proposed haptic control algorithm is as follows:

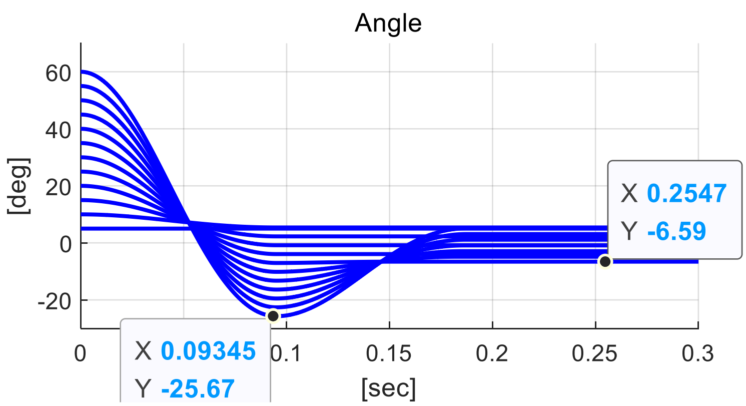

Figure 7.8 Return Test Result of Proposed Haptic Control Algorithm at 80kph

Using the proposed haptic control algorithm, the overshoot is 25.67deg and the maximum remaining angle is 6.59deg. The overshoot increased by about 9.5% and the maximum remaining angle increased by about 8.6%. The resolution and sampling time of the sensor reduce haptic rendering performance.

7.3. Vehicle Test Results for Haptic Control Algorithm

This section shows vehicle test results for haptic control algorithm. The vehicle test was conducted in the range of the vehicle speed at which the parameter update was performed. Table 4 shows the test cases in which the vehicle test was conducted. Figures 7.9 and 7.10 are vehicle test results in dry asphalt.

Table 2 Vehicle Test Case.

	Vehicle Speed	**Road Condition**
Test Case 1	45~49kph	Dry Asphalt (μ = 0.85)
Test Case 2	28~35kph	Dry Asphalt (μ = 0.85)
Test Case 3	28~36kph	Wet Asphalt (μ = 0.5)
Test Case 4	33~41kph	Wet Asphalt (μ = 0.5)
Test Case 5	32~40kph	Wet Asphalt with Slip (μ = 0.5)
Test Case 6	25kph	Dry Asphalt (μ = 0.85)

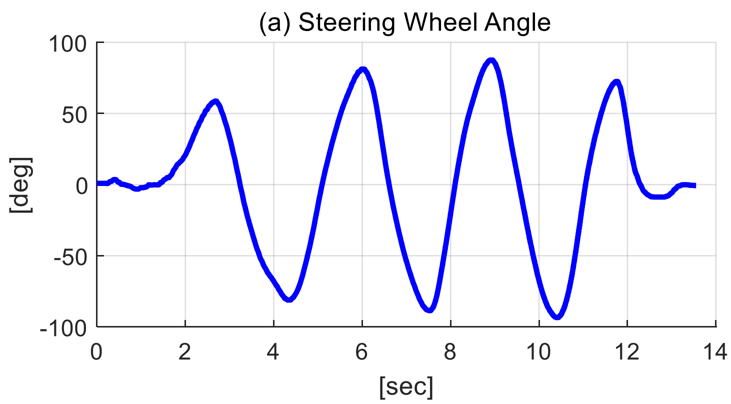

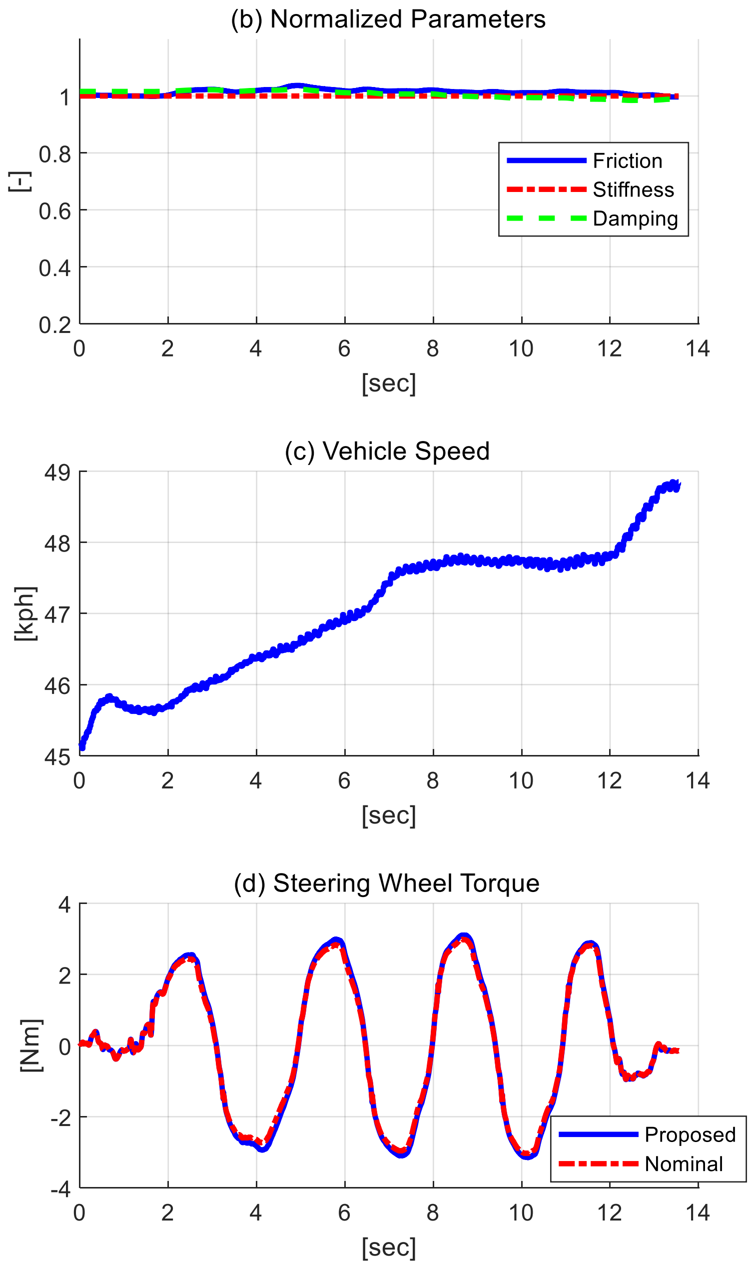

Figure 7.9 Vehicle Test Results of Case 1

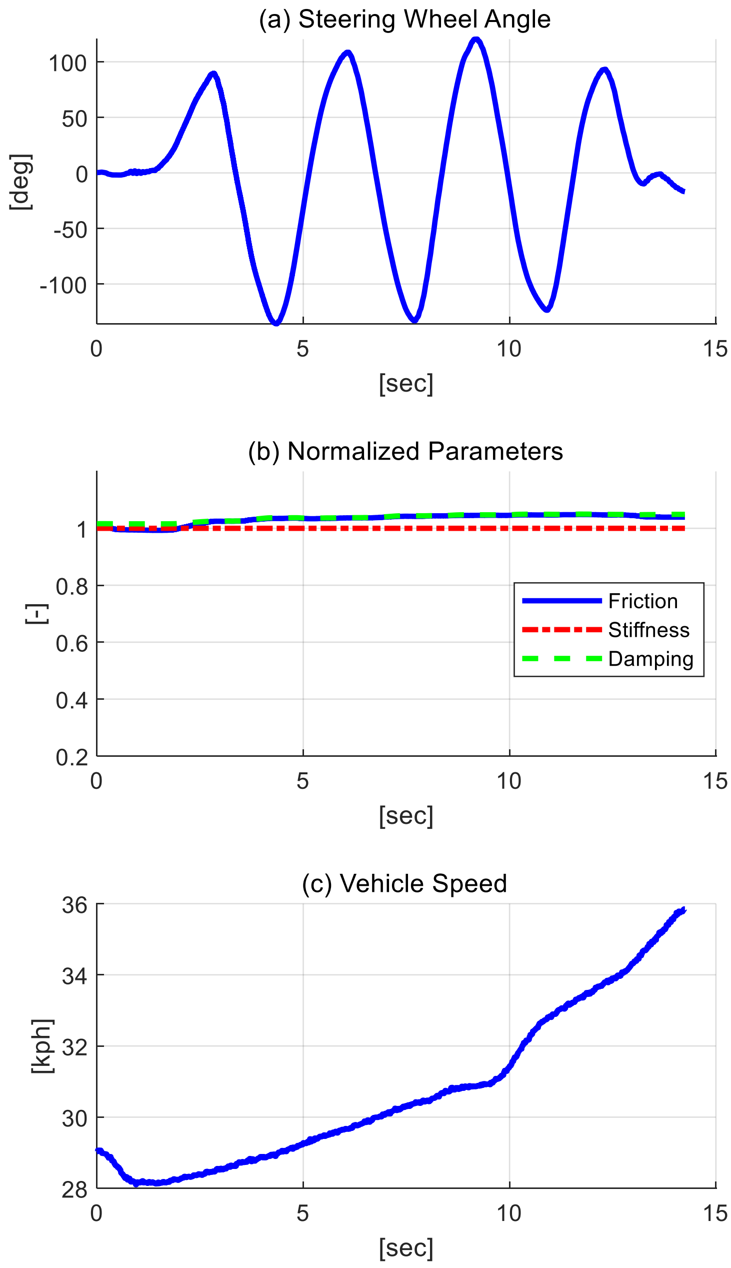
(a) Steering Wheel Angle
100
50
0
-50
-100
[deg]
0
5
10
15
[sec]
(b) Normalized Parameters
1
0.8
0.6
0.4
0.2
[-]
Friction
Stiffness
Damping
0
5
10
15
[sec]
(c) Vehicle Speed
36
34
32
30
28
[kph]
0
5
10
15
[sec]

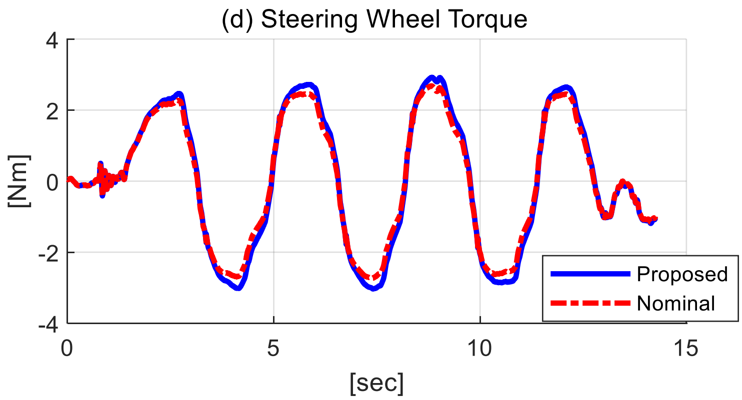

Figure 7.10 Vehicle Test Results of Case 2

The proposed algorithm has validated the rendering performance of the artificial steering model designed in dry asphalt. On the other hand, since Figure 7.11 and 7.12 are vehicle test in wet asphalt, the steering feel is reduced through parameter estimation. Figure 7.11 and 7.12 is as follows:

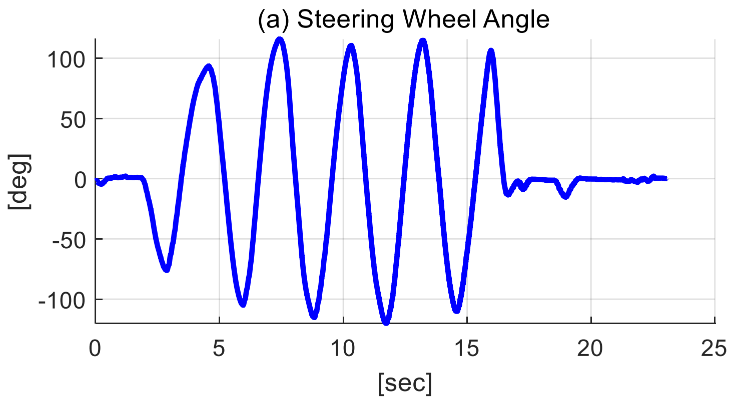

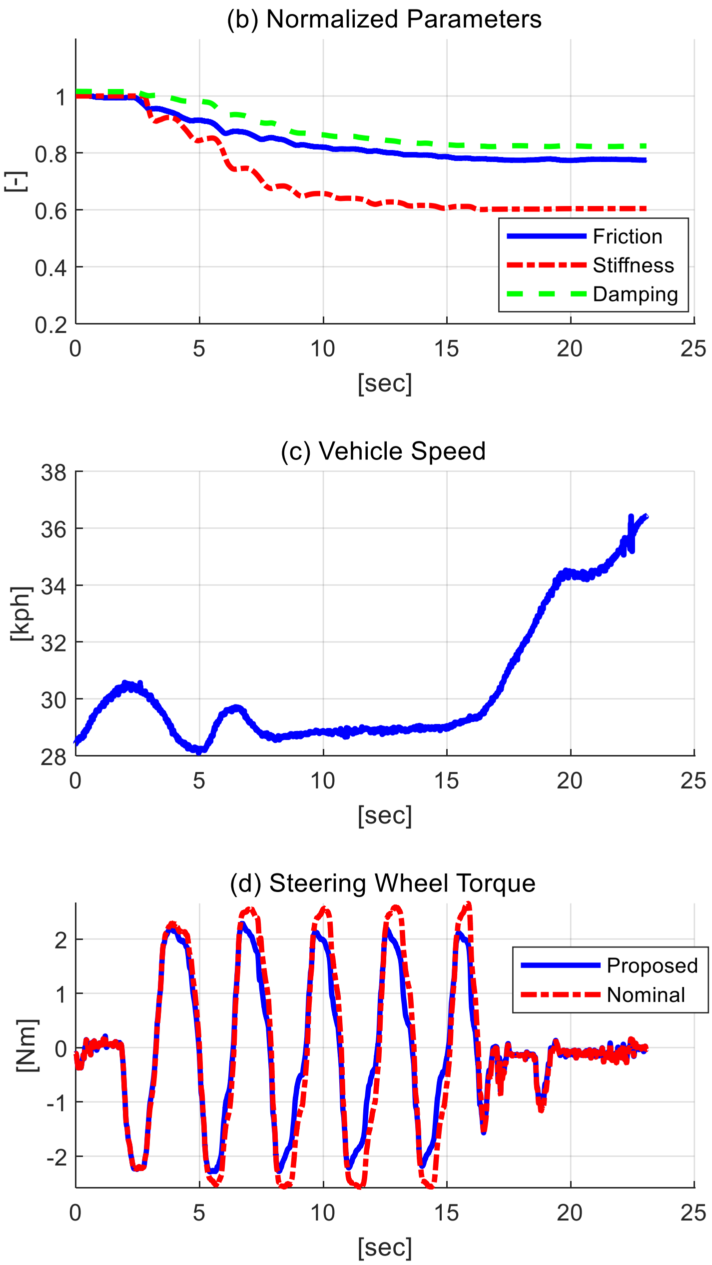

Figure 7.11 Vehicle Test Results of Case 3

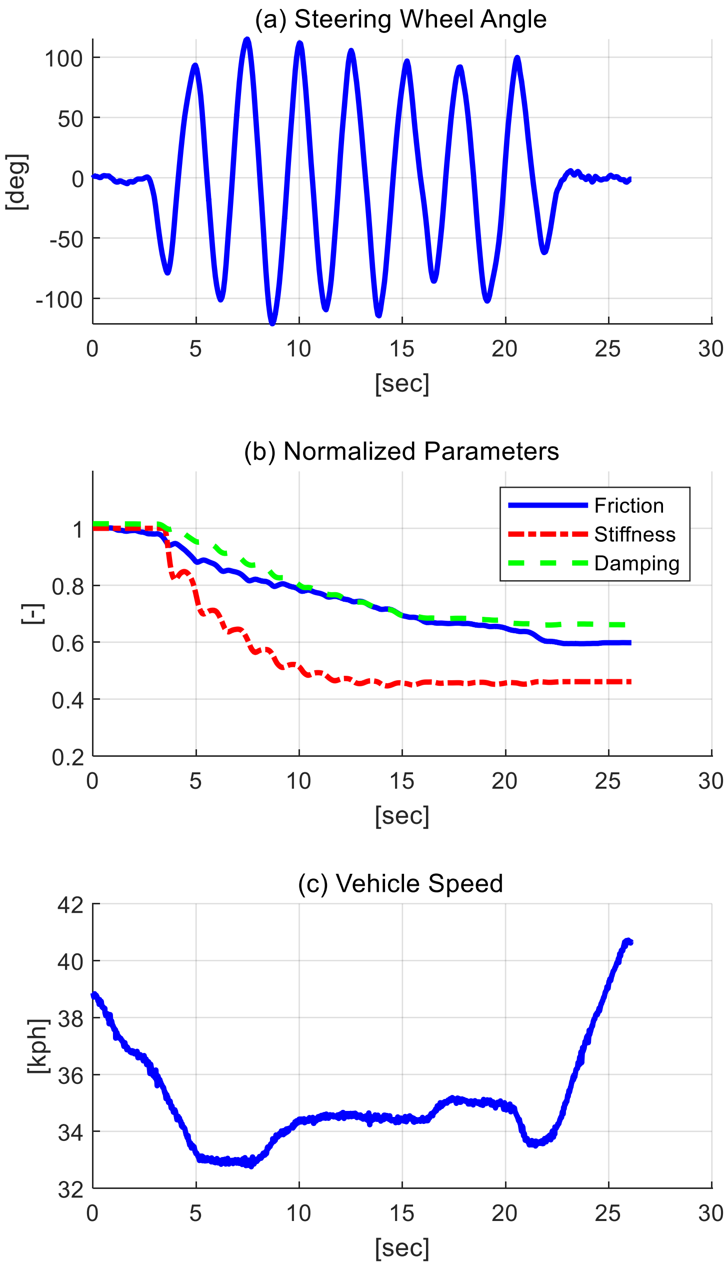
(a) Steering Wheel Angle
[deg]
100
50
0
-50
-100
0
5
10
15
20
25
30
[sec]
(b) Normalized Parameters
[-]
1
0.8
0.6
0.4
0.2
Friction
Stiffness
Damping
[sec]
(c) Vehicle Speed
[kph]
42
40
38
36
34
32
[sec]

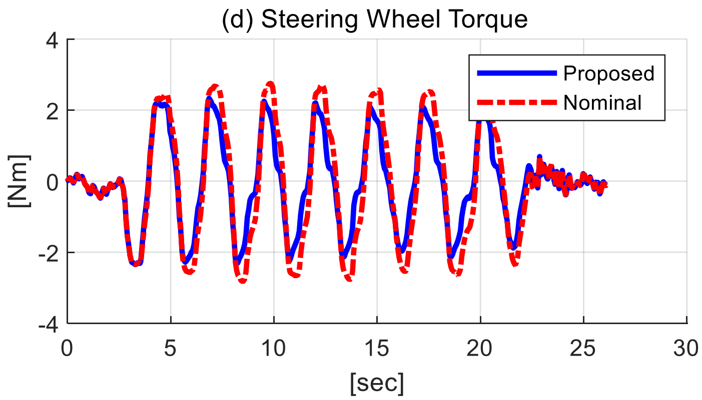

Figure 7.12 Vehicle Test Results of Case 4

In wet asphalt, the stiffness coefficient decreased because the friction coefficient was less than 0.5. And it is shown that each coefficient changes to a lower frequency. Figure 7.13 is the vehicle test results when the vehicle is unstable and slip occurs. Figure 7.13 is as follows:

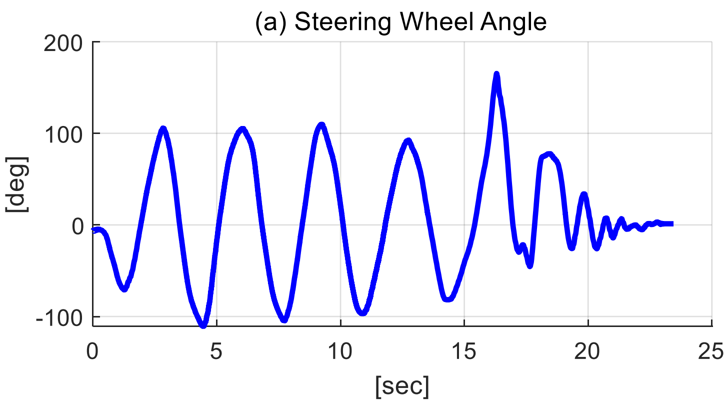

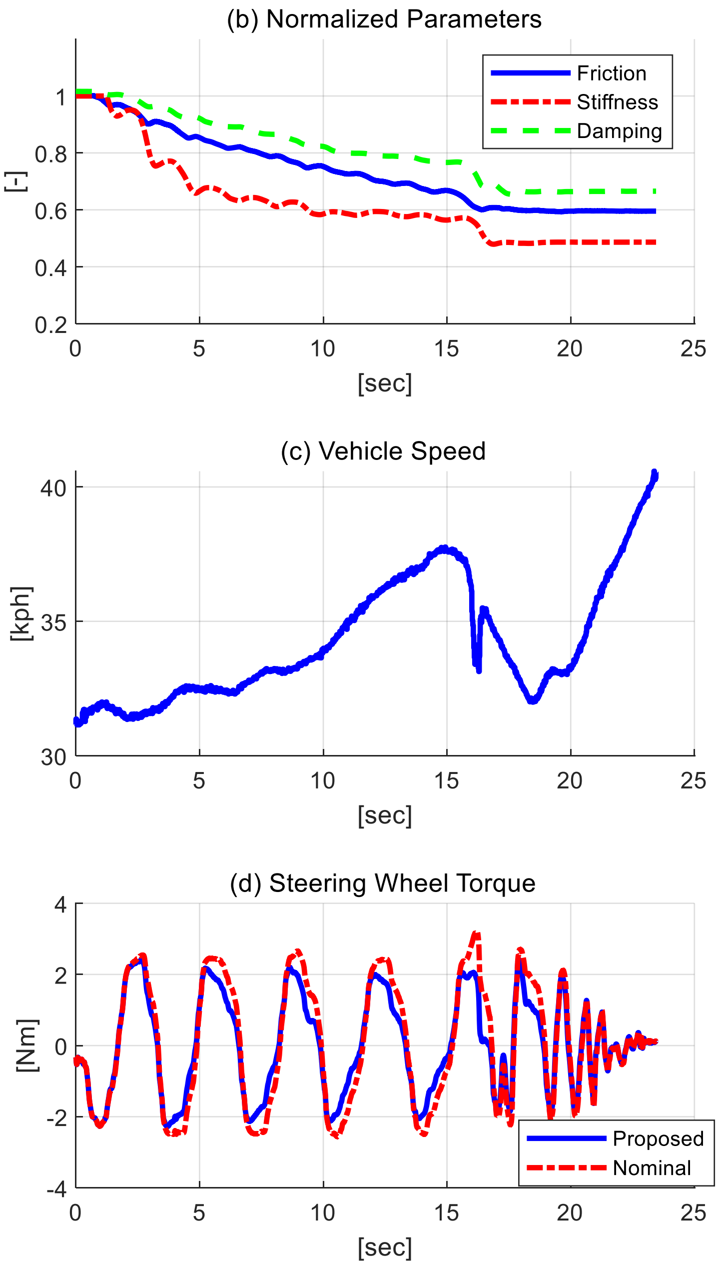

Figure 7.13 Vehicle Test Results of Case 5

Figure 7.14 is the return test results which is hands-off scenario. Figure 7.14 is as follows:

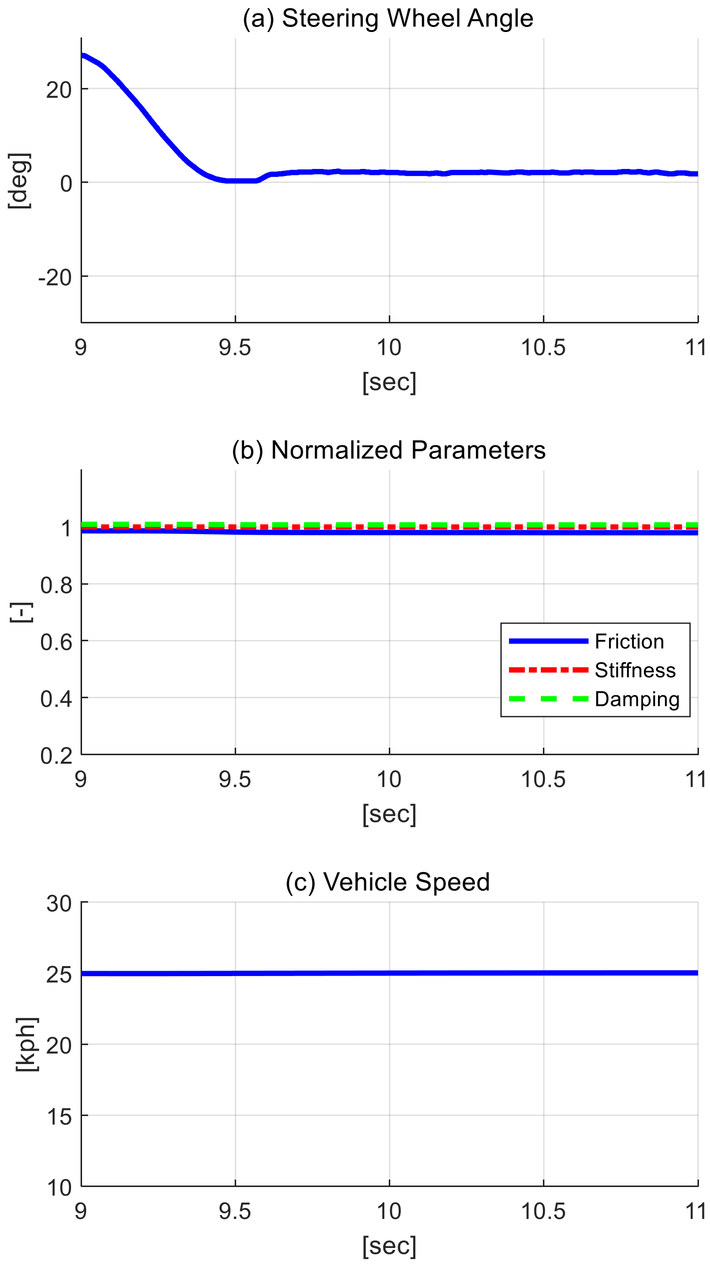

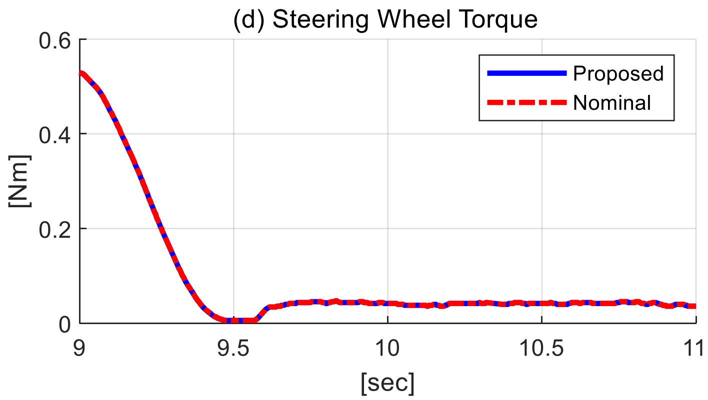

Figure 7.14 Vehicle Test Results for Case 6

Through the vehicle test results, the performance of the proposed haptic control algorithm was validated in a steer-by-wire vehicle.

The proposed algorithm is compared with the previously studied algorithms such as rack force-based algorithm and rack position tracking error-based algorithm. Since the low frequency range is the intended steering feel, the algorithms were tuned so that the steering was the same at the low frequency. Based on test case 5, comparative analysis was conducted offline. Figure 7.15 is the comparison between previously studied algorithms.

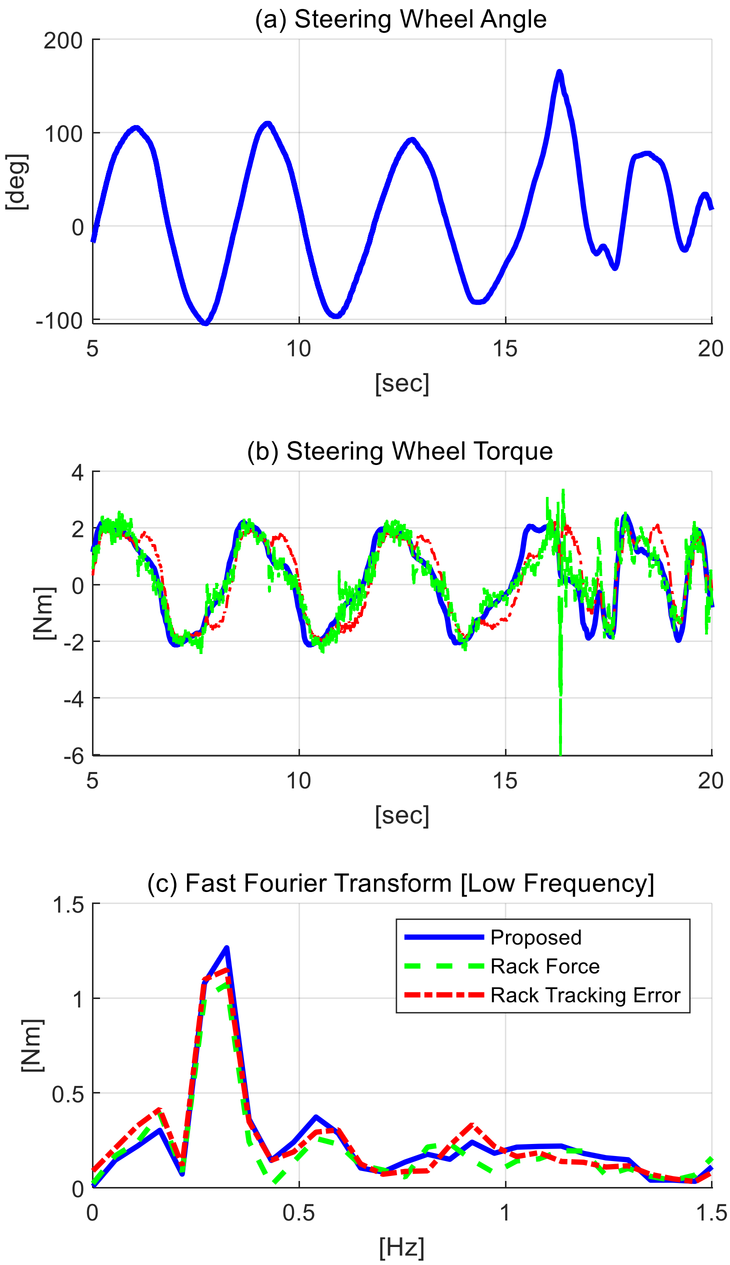

(a) Steering Wheel Angle
200
100
0
-100
[deg]
5
10
15
20
[sec]
(b) Steering Wheel Torque
4
2
0
-2
-4
-6
[Nm]
5
10
15
20
[sec]
(c) Fast Fourier Transform [Low Frequency]
1.5
1
0.5
0
[Nm]
0
0.5
1
1.5
[Hz]
Proposed
Rack Force
Rack Tracking Error

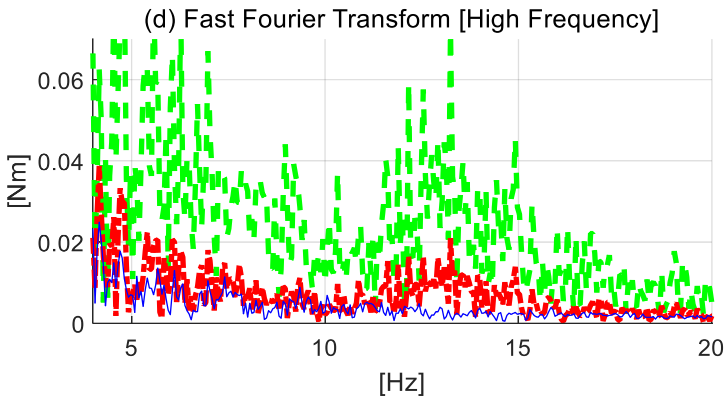

Figure 7.15 Performance Comparison using Vehicle Test Result

Even though similar steering feel is generated, the proposed algorithm has a smaller torque in the high frequency domain, which adversely affects the steering feel. In summary, the stable steering feel generation performance of the proposed haptic control algorithm was verified.

Chapter 8 Conclusion and Future works

This dissertation describes a haptic control algorithm under various driving conditions. In this study, we focus on developing a haptic control algorithm by considering quantization and sampling rate of the angle sensor to secure the stable and high performance of steering feel generation. The proposed algorithm consisted of the following three steps: artificial steering model, a lateral load model-based parameter estimation algorithm in a rack system, and a passive condition-based parameter update algorithm.

The artificial steering model was developed by separating the driving region and stopping region. In the case of the driving region, optimization has been conducted to satisfy the target torque defined in the weave test and transition test. In the case of the stopping region, the dynamics were designed in reverse-based on the vehicle test data.

Tire lateral force was analyzed to transmit road surface information to the driver. Tire lateral force was assumed as a lateral load model of the rack system. Parameters of the lateral load model were estimated based on the Kalman filter, and through this, the change of road surface conditions at low frequency was indirectly estimated.

Passivity conditions were derived through energy analysis to generate a stable steering feel, When the passivity condition is satisfied, there is no unstable behavior or limit cycles. By designing a parameter update algorithm based on the passivity conditions, stable steering feel generation performance has been validated even if the artificial steering model changes in real time.

The performance of the proposed haptic control algorithm was evaluated by performing simulations and vehicle tests under various steering and road conditions. By reflecting the change in road conditions, stable steering feel generation performance was validated, and the torque in the high frequency domain, which adversely affects the steering feel was reduced compared to previous studies.

Our future plans for the haptic control of steer-by-wire systems can be summarized into three major aspects. The first is to modify the artificial steering model. Since the functions constituting the steering model are not optimal, these functions do not completely satisfy the objective evaluation index. It is necessary to design an optimal artificial steering model. The second is to improve the steering wheel angular velocity estimation method. A finite difference method and infinite impulse response filter used in this dissertation are not optimal methods for estimating the angular velocity. The plan is to study various estimation methods. The last is the advancement of the lateral load model. It is expected that by advancing the lateral load model, not only road friction but also changes of various road surface conditions can be transmitted to the driver.

Bibliography

13674-1:, I. (2003). Road vehicles–test method for the quantification of on-centre handling–Part 1: weave test, International Organization for Standardization Geneva.

AHMADKHANLOU, F., et al. (2006). Magnetorheological fluid based automotive steer-by-wire systems. Smart Structures and Materials 2006: Industrial and Commercial Applications of Smart Structures Technologies, International Society for Optics and Photonics.

ASAI, S., et al. (2004). Development of a steer-by-wire system with force feedback using a disturbance observer, SAE Technical Paper.

BADAWY, A., et al. (1999). Modeling and analysis of an electric power steering system, SAE Technical Paper.

BAJéINCA, N., et al. (2003). Haptic control for steer-by-wire systems. Proceedings 2003 IEEE/RSJ International Conference on Intelligent Robots and Systems (IROS 2003)(Cat. No. 03CH37453), IEEE.

BALACHANDRAN, A. and J. C. GERDES (2013). "Artificial steering feel design for steer-by-wire vehicles." IFAC Proceedings Volumes **46**(21): 404-409.

BALACHANDRAN, A. and J. C. GERDES (2014). "Designing steering feel for steer-by-wire vehicles using objective measures." IEEE/ASME Transactions on Mechatronics **20**(1): 373-383.

BERNARD, J. E. and C. L. CLOVER (1995). "Tire modeling for low-speed and high-speed calculations." SAE transactions: 474-483.

BOULES, N., et al. (2002). Torque ripple free electric power steering, Google Patents.

CHEON, D. and K. NAM (2017). "Steering torque control using variable impedance models for a steer-by-wire system." International Journal of Automotive Technology **18**(2): 263-270.

COLLIER-HALLMAN, S. J. and A. CHANDY (2000). Electric power steering control with torque ripple and road disturbance damper, Google Patents.

COLONNESE, N. and A. OKAMURA (2016). "Stability and quantization-error analysis of haptic rendering of virtual stiffness and damping." The International Journal of Robotics Research **35**(9): 1103-1120.

COLONNESE, N., et al. (2014). Closed-loop stiffness and damping accuracy of impedance-type haptic displays. 2014 IEEE Haptics Symposium (HAPTICS), IEEE.

DANG, J., et al. (2014). "Optimal design of on-center steering force characteristic based on correlations between subjective and objective evaluations." SAE International Journal of Passenger Cars-Mechanical Systems **7**(2014-01-0137): 992-1001.

DANNøHL, C., et al. (2012). "H∞-control of a rack-assisted electric power steering system." Vehicle System Dynamics **50**(4): 527-544.

DI CAIRANO, S., et al. (2012). "Vehicle yaw stability control by coordinated active front steering and differential braking in the tire sideslip angles domain." IEEE Transactions on Control Systems Technology **21**(4): 1236-1248.

DIOLAITI, N., et al. (2005). A criterion for the passivity of haptic devices. Proceedings of the 2005 IEEE International Conference on Robotics and Automation, IEEE.

DIOLAITI, N., et al. (2006). "Stability of haptic rendering: Discretization, quantization, time delay, and coulomb effects." IEEE Transactions on Robotics **22**(2): 256-268.

DISCENZO, F. M. (2000). Steer by wire system with feedback, Google Patents.

DUGOFF, H., et al. (1969). Tire performance characteristics affecting vehicle response to steering and braking control inputs.

FALCONE, P., et al. (2008). "MPC-based yaw and lateral stabilisation via active front steering and braking." Vehicle System Dynamics **46**(S1): 611-628.

FANKEM, S. and S. MþLLER (2014). "A new model to compute the desired steering torque for steer-by-wire vehicles and driving simulators." Vehicle System Dynamics **52**(sup1): 251-271.

FORSYTH, B. A. and K. E. MACLEAN (2005). "Predictive haptic guidance: Intelligent user assistance for the control of dynamic tasks." IEEE transactions on visualization and computer graphics **12**(1): 103-113.

GAZIT, R. Y. (2015). Steering wheels for vehicle control in manual and autonomous driving, Google Patents.

GIL, J. J., et al. (2004). "Stability analysis of a 1 dof haptic interface using the routh-hurwitz criterion." IEEE Transactions on Control Systems Technology **12**(4): 583-588.

GIL, J. J., et al. (2009). "Stability boundary for haptic rendering: Influence of damping and delay." Journal of Computing and Information Science in Engineering **9**(1).

HSU, Y.-H. J. and J. C. GERDES (2008). "The predictive nature of pneumatic trail: Tire slip angle and peak force estimation using steering torque." Proc. AVEC08 **8085**.

JIANG, Y., et al. (2015). Studies on influencing factors of driver steering torque feedback, SAE Technical Paper.

KAUFMANN, T. W. and M. D. BYERS (2002). Steer-by-wire system, Google Patents.

KIM, J.-H. and J.-B. SONG (2002). "Control logic for an electric power steering system using assist motor." Mechatronics **12**(3): 447-459.

KIM, K., et al. (2020). "Adaptive Sliding Mode Control of Rack Position Tracking System for Steer-by-Wire Vehicles." IEEE Access **8**: 163483-163500.

KISSAI, M., et al. (2017). A new linear tire model with varying parameters. 2017 2nd IEEE International Conference on Intelligent Transportation Engineering (ICITE), IEEE.

KLIER, W., et al. (2004). Concept and functionality of the active front steering system, SAE technical paper.

KOBAYASHI, H., et al. (2011). Control apparatus for electric power steering apparatus, Google Patents.

KOKOTOVIC, V. V., et al. (1999). "Electro hydraulic power steering system." SAE transactions: 661-671.

LAWRENCE, D. A. (1992). Designing teleoperator architectures for transparency. Proceedings 1992 IEEE International Conference on Robotics and Automation, IEEE Computer Society.

LAWRENCE, D. A. (1993). "Stability and transparency in bilateral teleoperation." IEEE transactions on robotics and automation **9**(5): 624-637.

LEE, J., et al. (2017). Steering wheel torque control of steer-by-wire system for steering feel, SAE Technical Paper.

LEE, J., et al. (2018). Control of Steer by Wire System for Reference Steering Wheel Torque Tracking and Return-Ability, SAE Technical Paper.

LEE, J., et al. (2020). "Haptic control of steer-by-wire systems for tracking of target steering feedback torque." Proceedings of the Institution of Mechanical Engineers, Part D: Journal of Automobile Engineering **234**(5): 1389-1401.

MEIJAARD, J. and A. SCHWAB (2006). Linearized equations for an extended bicycle model. III European Conference on Computational Mechanics, Springer.

NAM, K., et al. (2012). "Advanced motion control of electric vehicles based on robust lateral tire force control via active front steering." IEEE/ASME Transactions on Mechatronics **19**(1): 289-299.

NIEMEYER, G. and J.-J. SLOTINE (1991). "Stable adaptive teleoperation." IEEE Journal of oceanic engineering **16**(1): 152-162.

NORMAN, K. D. (1984). "Objective evaluation of on-center handling performance." SAE transactions: 380-392.

NORO, Y., et al. (1997). Electric power steering apparatus having a phase compensation section, Google Patents.

NYBACKA, M., et al. (2014). "Links between subjective assessments and objective metrics for steering, and evaluation of driver ratings." Vehicle System Dynamics **52**(sup1): 31-50.

ODENTHAL, D., et al. (2002). How to make steer-by-wire feel like power steering. Proc. 15th IFAC World Congress on Automatic Control.

OH, S.-W., et al. (2004). "The design of a controller for the steer-by-wire system." JSME International Journal Series C Mechanical Systems, Machine Elements and Manufacturing **47**(3): 896-907.

PACEJKA, H. (2005). Tire and vehicle dynamics, Elsevier.

PACEJKA, H. B. (1995). "Modeling of the pneumatic tyre and its impact on vehicle dynamic behaviour."

PACEJKA, H. B. and E. BAKKER (1992). "The magic formula tyre model." Vehicle System Dynamics **21**(S1): 1-18.

PARK, J. and O. KHATIB (2006). "A haptic teleoperation approach based on contact force control." The International Journal of Robotics Research **25**(5-6): 575-591.

PARK, Y. and I. JUNG (2001). "Semi-active steering wheel for steer-by-wire system." SAE transactions: 2528-2535.

PERETTI, L. and M. ZIGLIOTTO (2006). "A force feedback system for steer-by-wire applications based on low-cost MR fluids-design hints."

RADAMIS, M. and B. ZHENG (2003). Torque sensor backup in a steer-by-wire system, Google Patents.

REN, B., et al. (2016). "MPC-based yaw stability control in in-wheel-motored EV via active front steering and motor torque distribution." Mechatronics **38**: 103-114.

ROGERS, C., et al. (2003). High efficiency automotive hydraulic power steering system, Google Patents.

SALAANI, M. K., et al. (2004). "Experimental steering feel performance measures." SAE transactions: 665-679.

SCICLUNA, K., et al. (2017). Torque feedback for steer-by-wire systems with rotor flux oriented PMSM. 2017 19th International Conference on Electrical Drives and Power Electronics (EDPE), IEEE.

SETLUR, P., et al. (2006). "A trajectory tracking steer-by-wire control system for ground vehicles." IEEE Transactions on vehicular technology **55**(1): 76-85.

SHIMIZU, Y. (1989). Electric power steering system for vehicles, Google Patents.

SIERRA, C., et al. (2006). "Cornering stiffness estimation based on vehicle lateral dynamics." Vehicle System Dynamics **44**(sup1): 24-38.

SPALL, J. C. and K. D. WALL (1984). "Asymptotic distribution theory for the Kalman filter state estimator." Communications in Statistics-Theory and Methods **13**(16): 1981-2003.

SPENCER JR, B., et al. (1997). "Phenomenological model for magnetorheological dampers." Journal of engineering mechanics **123**(3): 230-238.

STOLTE, R. C. (1957). Hydraulic power steering mechanism, Google Patents.

SUZUKI, K., et al. (1995). Integrated electro-hydraulic power steering system with low electric energy consumption, SAE Technical Paper.

SVENDENIUS, J. (2003). Tire models for use in braking applications, Department of Automatic Control, Lund Institute of Technology Masters, Lund ….

SVENDENIUS, J. and B. WITTENMARK (2003). Brush tire model with increased flexibility. 2003 European Control Conference (ECC), IEEE.

WU, X., et al. (2016). "Two-port network based bilateral control of a steer-bywire system." International Journal of Automotive Technology **17**(6): 983-990.

ZHANG, L. and G. STEPAN (2020). "Bifurcations in basic models of delayed force control." Nonlinear Dynamics **99**(1): 99-108.

ZHENG, B. and S. ANWAR (2009). "Yaw stability control of a steer-by-wire equipped vehicle via active front wheel steering." Mechatronics **19**(6): 799-804.

ZHENG, B. and B. LENART (2006). Oversteering/understeering compensation with active front steering using steer by wire technology, Google Patents.

박영대, et al. (2019). "조타감 성능 목표 달성을 위한 모델 기반 MDPS 제어맵 최적화 설계." Transactions of the Korean Society of Automotive Engineers **27**(10): 755-761.

초 록

도로 노면 상태 업데이트 및 인공 조향 모델을 활용한 스티어 바이 와이어 시스템 햅틱 제어

본 논문은 스티어 바이 와이어 (SBW) 시스템에서 조향감 재현을 하기 위한 햅틱 제어 알고리즘의 개발을 중점으로 한다. 이 연구에서는 조향각 센서의 양자화, 샘플링 주파수를 고려하여 안정적인 렌더링 성능을 확보하는 것을 목표로 한다. 햅틱 제어 알고리즘은 다음 세단계로 구성된다. 가상의 스티어링 모델과 랙 시스템에서의 횡하중 모델 기반 파라미터 추정 알고리즘, 수동성 조건 기반 파라미터 업데이트 알고리즘을 제안한다.

가상의 스티어링 모델은 주행 영역과 정차 영역을 분리하여 개발한다. 주행 영역에 경우 다양한 단조증가 함수를 정의하여 스티어링 시스템을 모델링하였다. 정현파(Weave Test) 및 등속 스티어링(Transition Test) 입력 시험에서 정의된 목표 토크를 만족시킬 수 있도록 최적화를 수행한다. 정차 영역에 경우 차량 실험 데이터 기반으로 다이나믹스를 역으로 설계하였다.

노면 정보를 운전자에게 전달하기 위하여 타이어 횡력 분석을 기반으로 한 횡하중 모델을 가정하였다. 칼만 필터 기반으로 횡하중 모델의 파라미터를 추정하였고 이를 통해 낮은 주파수의 노면 정보 변화를 간접적으로 추정하는 알고리즘을 제안하고자 한다.

안정적인 조향감 재현을 위하여 에너지 분석을 통해 수동성

조건을 도출되었다. 수동성 조건을 만족하면 시스템이 에너지를 항상 소모하기 때문에 불안정한 움직임이나 극한 주기 궤도가 발생하지 않는다. 이러한 수동성 조건을 기반으로 파라미터 업데이트 알고리즘을 설계하여 가상의 스티어링 모델이 실시간으로 변하더라도 안정적인 조향감 재현 성능을 확보하였다.

제안된 햅틱 제어 알고리즘의 성능은 다양한 조향 조건 및 도로 조건에서 시뮬레이션과 실차 실험을 수행하여 평가되었다. 도로 조건의 변화를 반영하여 안정적인 조향감 재현 성능을 확인하였고 기존의 조향감 재현 알고리즘들과 비교하여 높은 주파수의 이질감이 감소한 것을 확인하였다.

주요어: 스티어 바이 와이어, 가상 스티어링 모델, 파라미터 추정, 수동성 조건, 햅틱 제어, 타이어 모델, 조향감 재현 알고리즘

학 번: 2017-30011